Prediction of Horizontal In-situ Stress in Shale Gas Reservoirs Based on Artificial Neural Networks and Conventional Rock Mechanics ——A Case Study on Longmaxi Formation in Southern Sichuan (China)

by
Yifan Du

A thesis submitted in partial fulfillment of the requirements for the degree of

Master of Science

in

Petroleum Engineering

Department of Civil and Environmental Engineering

University of Alberta

ABSTRACT

Shale gas is one of the most important unconventional fossil fuel resources. It is usually developed by horizontal drilling and hydraulic fracturing techniques. The in-situ stress magnitude distribution in a given shale gas field is a significant factor that should be considered by horizontal drilling and hydraulic fracturing. However, the accurate determination of in-situ stresses is normally hindered by the lack of experimental data. Aiming to address this issue, this thesis proposes a method of combining artificial intelligence and conventional rock mechanics to predict the in-situ stress magnitudes in a given shale gas reservoir based on the logging data. Since the experimental in-situ stress data are not sufficiently large to serve as the training dataset, this thesis selects the data in two wells for which the calculated in-situ stress magnitudes are in good agreement with the measured in-situ stress magnitudes as the training samples. Empirical rock-mechanics equations are used to generate more training data based on the data collected from these two wells. Then, a 4-layer artificial neural network model is established to predict the magnitudes of horizontal in-situ stresses in other wells. The results show that the predicted maximum horizontal in-situ stress magnitudes and predicted minimum horizontal in-situ stress magnitudes agree well with the measured data. Finally, a series of 3D maps showing the horizontal in-situ stress distributions in one shale gas reservoir in the Longmaxi formation of Sichuan (China) have been plotted by the newly developed neural network model.

DEDICATION

To my family and my friends.

ACKNOWLEDGMENTS

I would like to express my sincere gratitude and appreciation to my supervisor, Dr. Huazhou (Andy) Li, for his encouragement, support, patience, and guidance during my MSc program. I would also like to thank my examination committee chair, Dr. Bo Zhang, and my examination committee members, Dr. Nobuo Maeda and Dr. Hongbo Zeng, for their insightful comments and suggestions. In addition, I want to express my sincere thanks to Dr. Hucheng Deng, Dr. Jianhua He, and Dr. Chuangang Xiang for providing field data and technical assistance.

TABLE OF CONTENTS

LIST OF TABLES

LIST OF FIGURES

CHAPTER 1 INTRODUCTION

1.1 Research Background

With the depletion of conventional oil and gas reservoirs, unconventional shale gas reservoirs have become more important targets for exploration and development ever. Since shale is characterized by low porosity and low permeability, horizontal drilling and hydraulic fracturing have been widely used to exploit shale gas resources (Lian et al., 2015; Neuzil, 2019). The design and implementation of these engineering processes are greatly affected by the in-situ stress state of shale gas reservoirs. For example, the in-situ stress state helps determine the orientation of the horizontal well sections (Rasouli et al., 2011). In the hydraulic fracturing process, the in-situ stress state controls the shape, height, width, and direction of hydraulic fractures, thus posing a significant effect on the productivity of the created hydraulic fractures (Zhang et al., 2018). The magnitude of the horizontal in-situ stresses is a part of the in-situ stress state. Therefore, accurate evaluation of the horizontal in-situ stress magnitudes plays an essential role in the efficient exploitation of shale gas resources.

1.2 Literature Review

The in-situ stresses in a geological formation are generally comprised of coupled tectonic stress, gravitational stress, thermal stress, and pore pressure (Ju et al., 2017). The in-situ stress state in a geological formation is usually represented by vertical stress, maximum horizontal in-situ stress, and minimum horizontal in-situ stress (Lin et al., 2006; Matsuki

and Takeuchi, 1993).

There are many methods to evaluate the magnitudes of in-situ stresses, such as hydraulic fracturing, acoustic emission, and well logging (Haimson and Fairhurst, 1969; Seto et al., 1997; Thiercelin and Plumb, 1994). The hydraulic fracturing method can help to determine the in-situ stress based on the mini-frac test data. These data reflect the relationship between pressure and time during the fracturing process (Haimson and Fairhurst, 1969). However, we cannot conduct the mini-frac test in every well, making this method inapplicable sometimes. We can also obtain the in-situ stresses by analyzing the sonic characteristics of the measured elastic waves (Seto et al., 1999). The sonic emission method is very useful in measuring the magnitude of the in-situ stress in the deep formations. However, this method is expensive and cannot reflect the characteristics of the whole formation in a well. Based on the conventional logging data, some empirical calculation methods have been developed to determine the in-situ stresses (Thiercelin and Plumb, 1994). However, these empirical methods may lose their accuracy when being extrapolated to other conditions that are not considered in the model-building stage.

There are very few studies that explore the use of artificial neural network (ANN) models to predict the in-situ horizontal stresses. Recently, Abbas et al. (2020) developed an ANN model that could be used to predict the magnitudes of horizontal minimum in-situ stress. This method establishes a back-propagation (BP) neural network model by training it against the measured minimum horizontal in-situ stresses. The conventional well logging

data are the input data, including compressional wave transit times, shear wave transit times, density, total porosity, and gamma-ray. The minimum horizontal stress is measured by the leak-off and extended leak-off tests. Their study shows that the ANN model is able to reliably estimate a continuous profile of the minimum in-situ stress along the borehole.

1.3 Problem Statement

ANN is an emerging and promising method for in-situ stress magnitude evaluation. Admittedly, the performance of ANN highly depends on the quantity and quality of the data used for training the model. As for horizontal in-situ stress predictions, the training samples are usually obtained by interpreting the leak-off tests or triaxial rock tests. However, the leak-off tests and triaxial rock tests are expensive, highly limiting the amount of experimental in-situ stress data available for training the ANN model. This is particularly true for shale gas wells. Therefore, how to generate a sufficient number of experimental in-situ stress data is a problem that remains to be addressed.

1.4 Research Objectives and Technical Route

This thesis proposes a novel workflow to address the above problem. We focus on a shale gas field comprised of five wells. We find that the maximum and minimum horizontal stresses of two wells out of the five wells can be well predicted by empirical rock-mechanics correlations. This implies that we can possibly use the empirical correlations to generate a large database that includes continuous profiles of maximum and minimum horizontal stresses along the borehole. The large but artificially generated database is then

used to train the ANN model. Thus, the objective of this research is to propose a hybrid approach that can combine the empirical rock-mechanics equations and an ANN model to more accurately predict the maximum and minimum horizontal in-situ stresses in shale gas reservoirs.

1.5 Thesis Structure

There are five chapters in this thesis:

- **Chapter 1** introduces the research background with regard to the prediction of the in-situ horizontal stress magnitudes, literature review, problem statement, research objective, and thesis structure.
- **Chapter 2** shows the geological overview of the study area and introduces the data used in the research, which are the logging data and the measured in-situ stress data.
- **Chapter 3** presents the methodology developed to predict the in-situ horizontal stress in the study area.
- **Chapter 4** presents the research results and the related discussion. It is shown that the magnitudes of the in-situ stresses yielded by the trained ANN model are more accurate than the magnitudes of the in-situ stresses obtained by the conventional method. Finally, a series of 3D distribution maps of in-situ stress magnitudes in this study area are generated.
- **Chapter 5** summarizes the conclusions and gives recommendations for future

studies.

References

Abbas, A., Alsaba, M., Al, D., Dahm, H., Alhumairi, M. (2020). Determination of Minimum Horizontal Stress Magnitudes from Conventional Well Logging Data Using Artificial Neural Network. Paper ARMA 20–1495 presented at the 54th US Rock Mechanics/Geomechanics Symposium held in Golden, Colorado, USA.

Haimson, B., Fairhurst, C. (1969). In-situ Stress Determination at Great Depth by Means of Hydraulic Fracturing. Paper ARMA-69-0559 presented at the 11th U.S. Symposium on Rock Mechanics (USRMS), Berkeley, California.

Jenkins, A., Fathi, E, Belyadi, F. (2017). Stress Field Behavior Induced by Hydraulic Fracture in Shale Reservoirs: A Practical View on Cluster Spacing. Journal of Natural Gas Science and Engineering, 48(1), 186-196.

Ju, W., Shen, S., Qin, Y., Meng., Wu, C., Shen, Y., Yang, Z., Li, G., Li, C. (2017). In-Situ Stress State in the Linxing Region, Eastern Ordos Basin, China: Implications for Unconventional Gas Exploration and Production. Marine and Petroleum Geology, 86, 66-78.

Lian, Z., Yu, H., Lin, T., Guo, J. (2015). A Study on Casing Deformation Failure During Multistage Hydraulic Fracturing for the Stimulated Reservoir Volume of Horizontal

Shale Wells. Journal of Natural Gas Science and Engineering, 23, 538-546.

Lin, W., Kwaśniewski, M., Imamura, T., Matsuki, K. (2006). Determination of Three-Dimensional In-situ Stresses from Anelastic Strain Recovery Measurement of Cores at Great Depth. Tectonophysics, 426(2), 221-238.

Matsuki, K., Takeuchi, K. (1993). Three-dimensional In-situ Stress Determination by Anelastic Strain Recovery of a Rock Core. Paper ARMA-93-0637 presented at the 34th U.S. Symposium on Rock Mechanics (USRMS), Madison, Wisconsin.

Neuzil, C.E. (2019). Permeability of Clays and Shales. Annual Review of Earth and Planetary Sciences, 47, 247–73.

Rasouli, V., Pallikathekathil, Z. J., Mawuli, E. (2011). The Influence of Perturbed Stresses Near Faults on Drilling Strategy: A Case Study in Blacktip Field, North Australia. Journal of Petroleum Science and Engineering, 76, 37-50.

Seto, M., Nag, D.K., Vutukuri, V.S. (1999). In-Situ Rock Stress Measurement from Rock Cores Using the Acoustic Emission Method and Deformation Rate Analysis. Geotechnical and Geological Engineering, 17, 241-266.

Thiercelin, M.J., Plumb, R.A. (1994). Core-Based Prediction of Lithologic Stress Contrasts in East Texas Formations. SPE Formation Evaluation, 9 (04), 251–258.

Zhang, Y., Zhang, J., Yuan, B., Yin, S. (2018). In-situ Stress Controlling Hydraulic Fracture

Propagation and Fracture Breakdown Pressure. Journal of Petroleum Science and Engineering, 164, 164-173.

CHAPTER 2 OVERVIEW OF THE STUDY AREA AND DATA PREPARATION

2.1 Geological Overview of the Study Area

Y area studied in this thesis is located in the south of the Sichuan Basin. Its regional structure is located in the HY Mountain tectonic belt. Long 1 Member, the lower Marine shale of the Silurian Longmaxi Formation, is the main exploration strata. The lithology of Long 1 Member is black shale interbedded with thin siltstone layers. Long 1 Member is of deep-water shelf facies deposition with stable stratum thickness. These deep-water continental shelf subfacies can be further divided into seven types of sedimentary microfacies from top to bottom: rich silicon microbiological shale deep-water shelf facies, siliceous shale deep-water shelf sedimentary microfacies, clay siliceous shale deep-water shelf microfacies, siliceous clay shale deep-water shelf microfacies, calcareous clay shale deep-water shelf microfacies, calcium-rich clay shale deep-water shelf microfacies, and rich clay shale deep-water shelf microfacies.

2.2 Logging Data Preparation

This thesis uses the logging data of five wells (i.e., well Y1, well Y2, well Y3, well Y6, and well Y7) in the Y area, including XMAC logging (DTS), gamma-ray logging (GR), density logging (DEN), sonic logging (AC), and neutron logging (CNL). The interval of the logging data is 0.125 m, covering 4550 meters from the surface to the underground.

This thesis mainly focuses on the 1-9 layers of the target formation in the study area (**Figure 1-5**).

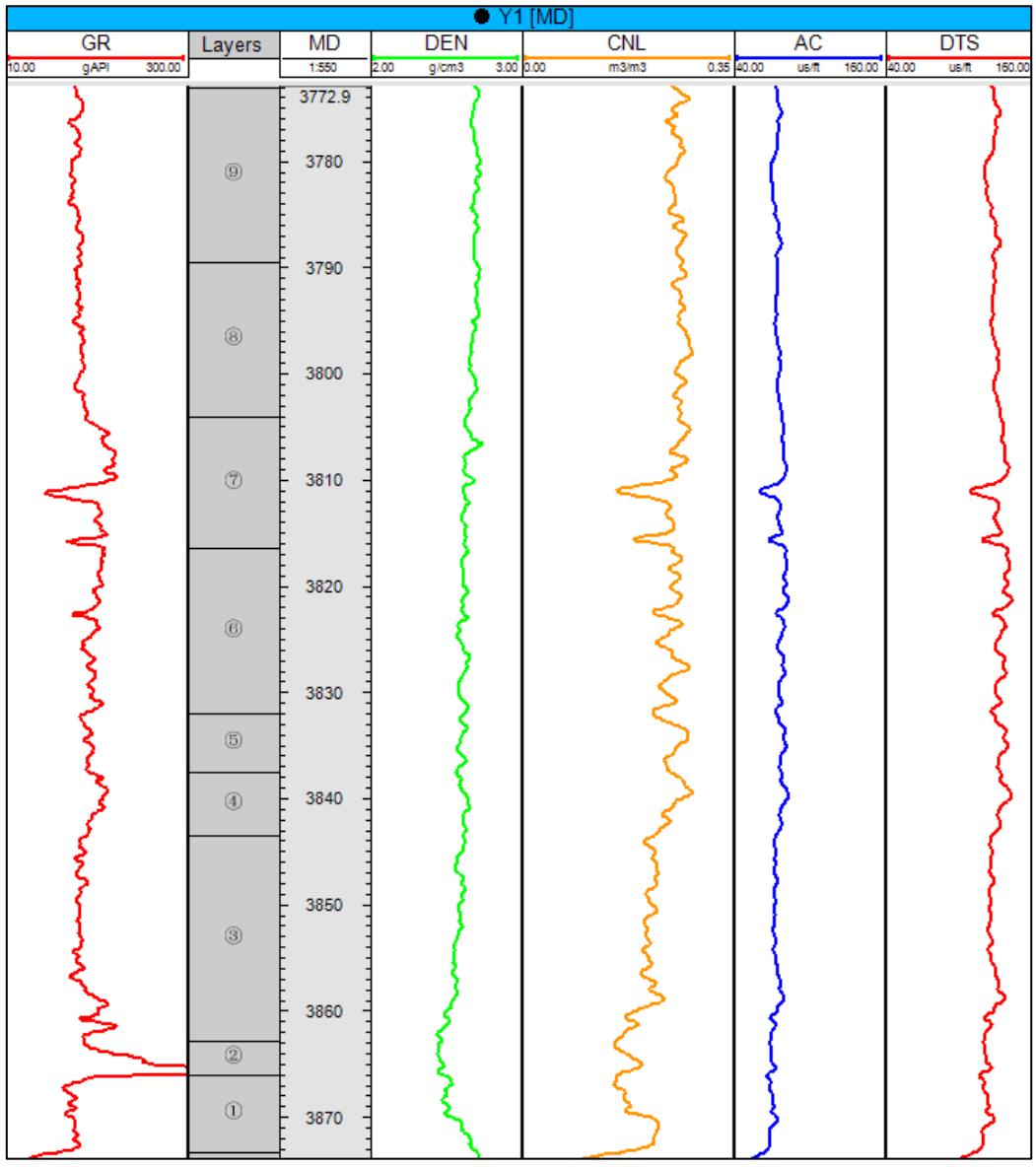

Figure 1 The logging data of well Y1 (GR: gamma-ray logging, MD: measured depth, DEN: density logging, CNL: neutron logging, AC: sonic logging, and DTS: XMAC logging).

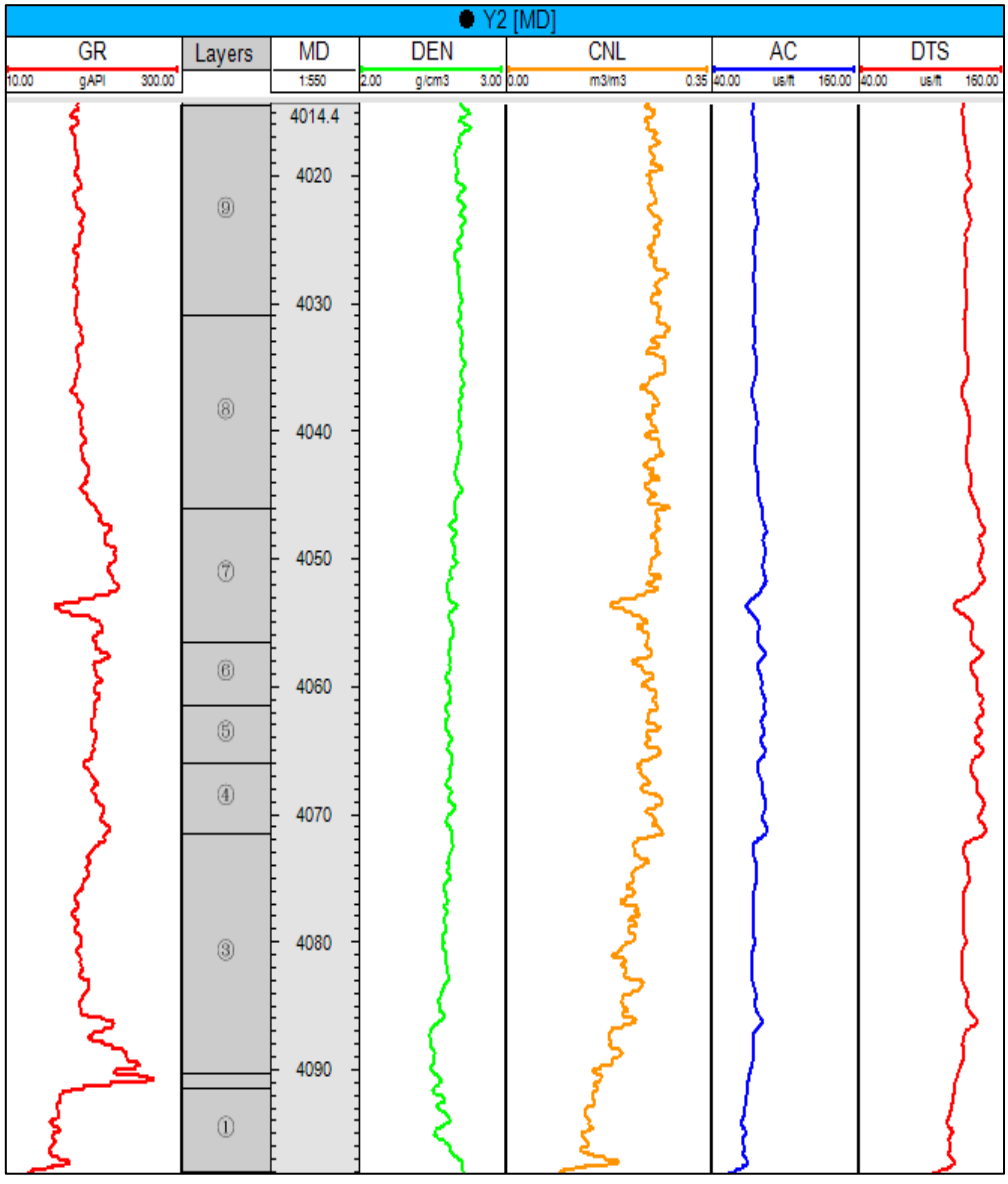

Figure 2 The logging data of well Y2.

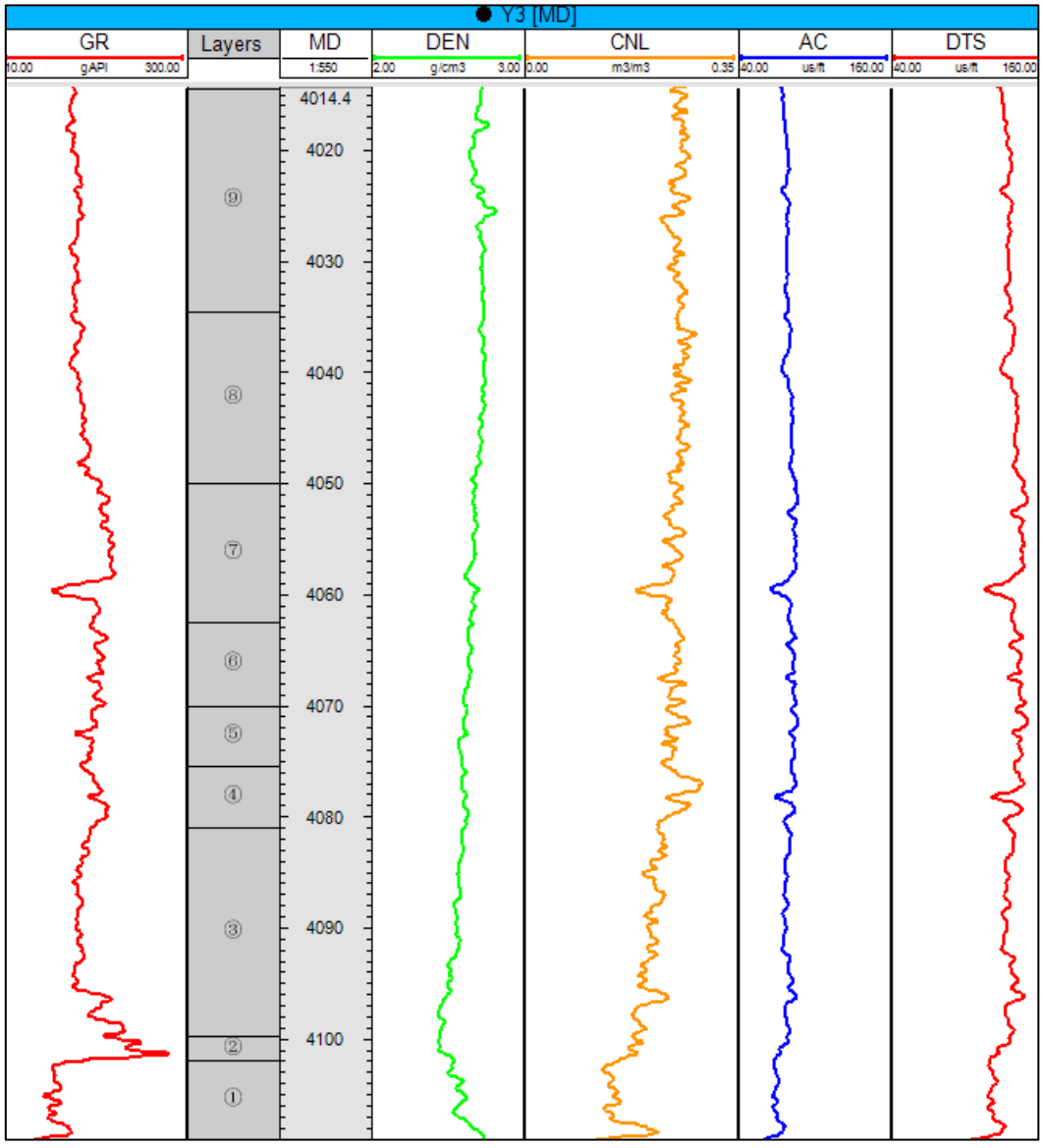

Figure 3 The logging data of well Y3.

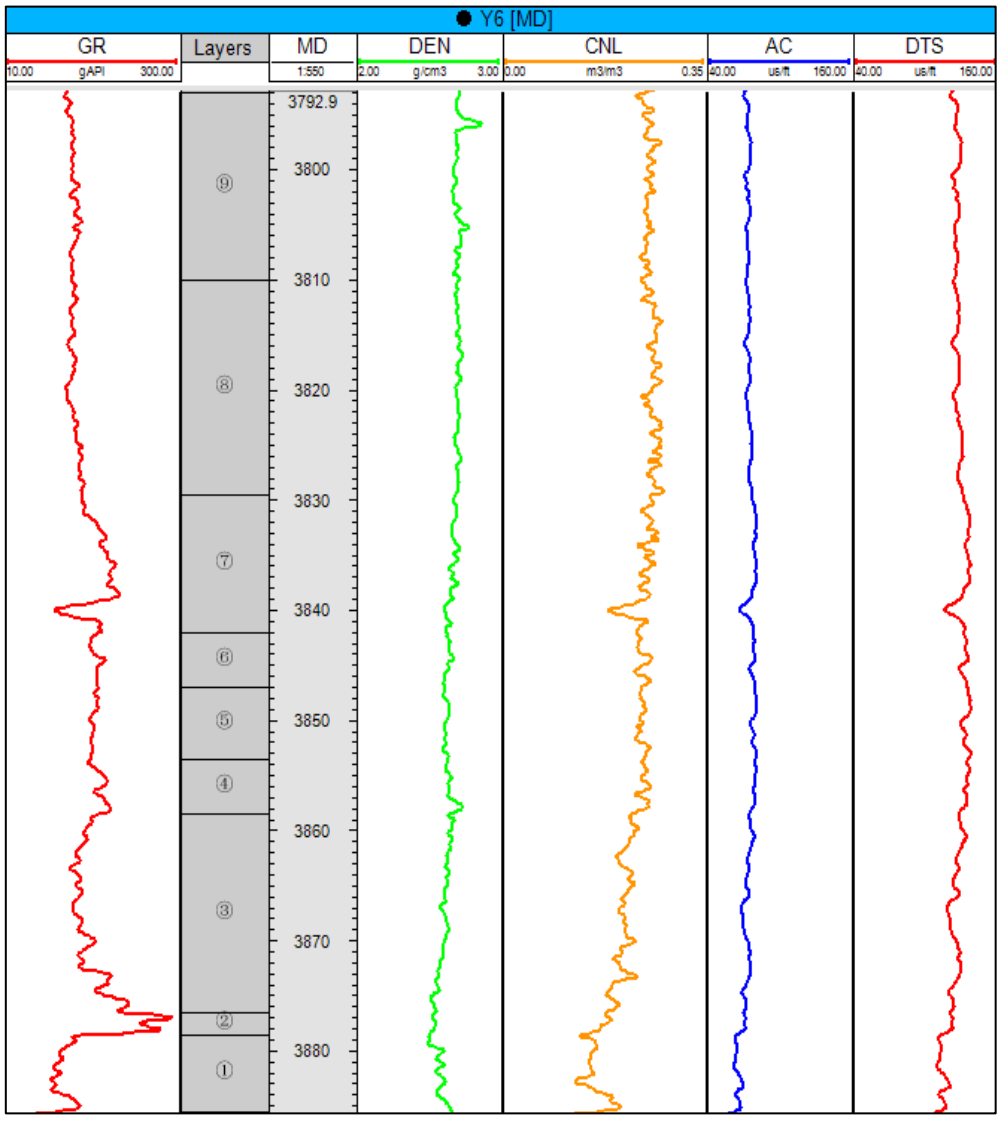

Figure 4 The logging data of well Y6.

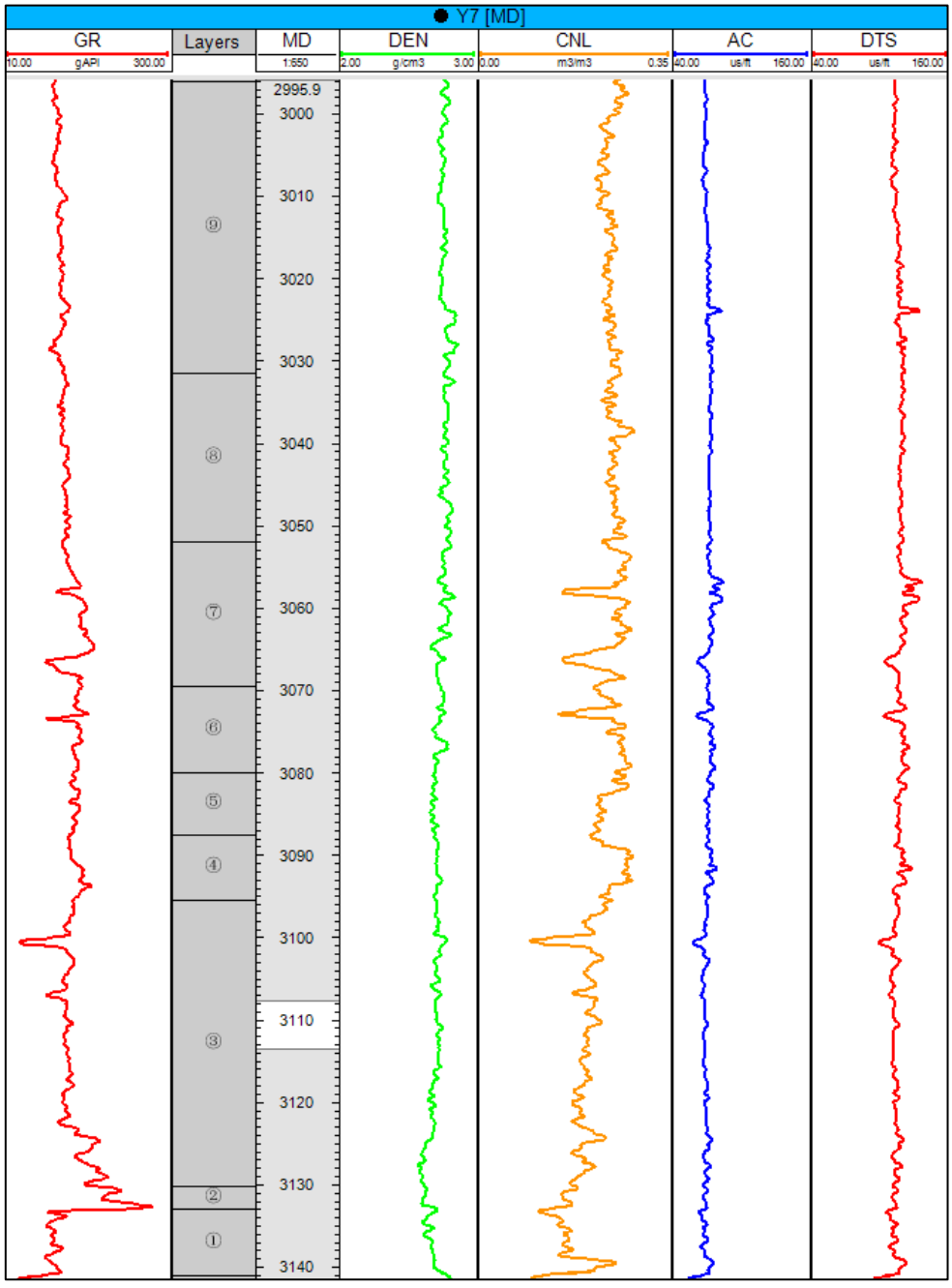

Figure 5 The logging data of well Y7.

2.3 Core Data Preparation

The core data used in this thesis are shown in Table 1, including the rock-mechanics parameters (Young's modulus and Poisson's ratio) and the in-situ horizontal stresses. In

Table 1, S_v represents vertical stress. The RTR-1000 triaxial rock testing machine and the SAEU2S acoustic emission system are applied to test the core samples in this study area. A total of 45 core samples are tested for Young's modulus and Poisson's ratio, while a total of 47 core samples are tested for the magnitudes of the maximum and minimum horizontal in-situ stresses (SH_{max} and SH_{min}).

Table 1 Core-related experimental data collected for the study area.

Well name	Layer	Depth/m	Poisson's ratio	Young's modulus, GPa	S_v, MPa	SH_{max}, MPa	SH_{min}, MPa
Y1	8	3802.66	0.279	24.667	93.19	97.72	86.16
Y1	7	3812.36	0.257	22.833	93.47	/	/
Y1	5	3834.76	0.250	27.114	94.10	99.06	88.94
Y1	4	3839.66	0.257	20.402	95.95	99.85	89.82
Y1	3	3844.26	0.267	24.243	96.79	104.39	86.76
Y1	3	3847.16	0.274	27.001	95.01	100.95	82.30
Y1	3	3854.06	0.285	30.588	95.09	100.70	90.59
Y1	3	3861.16	0.261	22.503	95.84	100.78	91.09
Y1	1	3868.36	0.264	22.333	96.10	100.12	92.01
Y2	9	4018.88	/	/	/	114.50	105.00
Y2	8	4036.28	/	/	/	109.00	99.90
Y2	7	4051.36	/	/	/	103.60	92.80
Y2	6	4057.81	0.215	28.460	/	109.90	103.60
Y2	6	4058.71	0.218	28.491	96.79	104.80	79.60
Y2	5	4064.11	0.232	28.667	/	105.30	98.00
Y2	4	4070.11	0.234	23.685	/	108.90	97.80
Y2	3	4082.21	0.265	26.400	/	113.70	102.40
Y2	3	4087.61	0.248	27.322	/	118.00	106.00
Y2	1	4093.21	0.230	28.300	/	117.40	100.00
Y3	4	4079.70	0.242	20.502	/	105.00	91.36
Y3	4	4079.90	0.242	20.825	/	107.11	92.28
Y3	4	4080.70	0.241	22.117	/	116.15	91.51
Y3	3	4081.50	0.240	23.461	/	106.47	91.40

Y3	3	4081.80	0.240	23.407	/	107.01	92.69
Y3	3	4089.50	0.252	22.111	88.03	105.95	80.54
Y3	3	4096.90	0.263	20.853	/	112.63	91.78
Y3	1	4102.70	0.242	26.502	/	116.87	94.65
Y3	1	4104.96	0.253	27.804	/	116.32	96.38
Y6	8	3828.56	0.240	29.105	94.44	97.95	93.61
Y6	7	3840.76	0.250	32.881	94.75	97.48	86.80
Y6	7	3842.76	0.246	28.988	88.03	100.19	76.67
Y6	5	3847.06	0.226	25.505	95.00	102.37	94.55
Y6	6	3848.06	0.218	26.644	94.89	100.94	89.55
Y6	4	3855.26	0.209	25.577	95.20	99.27	91.98
Y6	3	3864.76	0.250	29.331	96.06	106.68	93.64
Y6	3	3870.86	0.255	27.922	96.15	104.27	95.33
Y6	2	3876.06	0.259	26.719	96.75	104.06	93.85
Y6	2	3877.36	0.260	26.421	96.78	100.63	92.47
Y6	1	3882.56	0.280	27.425	96.92	103.68	93.53
Y7	9	3030.30	0.285	35.460	76.38	88.36	73.29
Y7	8	3046.10	0.292	24.011	74.90	81.07	64.97
Y7	7	3060.60	0.298	34.400	73.50	72.59	59.81
Y7	6	3072.30	0.279	25.600	76.47	94.87	77.00
Y7	5	3084.10	0.290	29.027	76.25	86.67	66.42
Y7	4	3094.70	0.318	34.326	77.56	92.57	73.22
Y7	3	3122.40	0.305	29.385	77.02	80.80	66.55
Y7	2	3130.80	0.279	29.726	78.76	97.44	78.79
Y7	1	3136.60	0.295	28.000	78.84	76.49	65.05

CHAPTER 3 METHODOLOGY

This chapter proposes a new methodology to predict the magnitudes of in-situ horizontal stresses based on ANN and conventional rock mechanics. Rock-mechanics parameters are obtained based on experimental data and well logging data. An ANN model has been formulated and trained. Eventually, the ANN model is used to predict a series of 3D distribution maps of the in-situ horizontal stresses in the study area.

Figure 6 shows the main workflow that has been developed in this study. The workflow mainly consists of the following steps:

1) We first retrieve cores from the five wells in the study area through coring operations. Next, we measure the rock-mechanics parameters (i.e., Young's modulus and Poisson's ratio) of the core samples. These measured Young's moduli and Poisson's ratios are the so-called static rock-mechanics parameters. We also measure the in-situ horizontal stresses using a triaxial test apparatus.

2) We select five input parameters that can influence the in-situ horizontal stresses from all the logging profiles obtained for the five wells. These parameters include gamma-ray logging (GR), density logging (DEN), sonic logging (AC), neutron logging (CNL), and depth (DEP). We can obtain shear wave slowness based on the DTS logging and compressional wave slowness based on the AC logging. Based on the shear wave slowness and compressional wave slowness, we can again

calculate Young's moduli and Poisson's ratios. These Young's moduli and Poisson's ratios obtained based on the interpretation of well logging data are the so-called dynamic rock-mechanics parameters. We then calculate the in-situ horizontal stresses using an empirical model.

3) Next, we compare the measured horizontal in-situ stresses against the ones calculated using an empirical rock-mechanics model. From the calculation results, we find that there are two wells for which the measured horizontal in-situ stresses agree well with the ones calculated using the empirical model. To address the above problem that normally it is expensive to measure the in-situ horizontal stresses using the retrieved core samples and there are thus insufficient experimental data, we generate more pseudo-experimental data of in-situ horizontal stresses by using the empirical model. These pseudo-experimental data are subsequently used to train the ANN model.

4) We predict the in-situ horizontal stresses in the other three wells using the trained ANN models and examine the model performance by comparing the calculated ones against the measured ones. It is found that the trained ANN model performs well in predicting the in-situ horizontal stresses in the other three wells.

5) In addition, we build a 3D geological model based on the stratigraphic data collected for this study area. By coupling with the well logging data, we obtain 3D

logging distribution models. On the basis of the 3D logging distribution model, we apply the developed ANN model to predict the 3D in-situ horizontal stress distributions across the reservoir. Such 3D distribution maps will be highly useful for guiding the drilling and hydraulic fracturing operations in the study area.

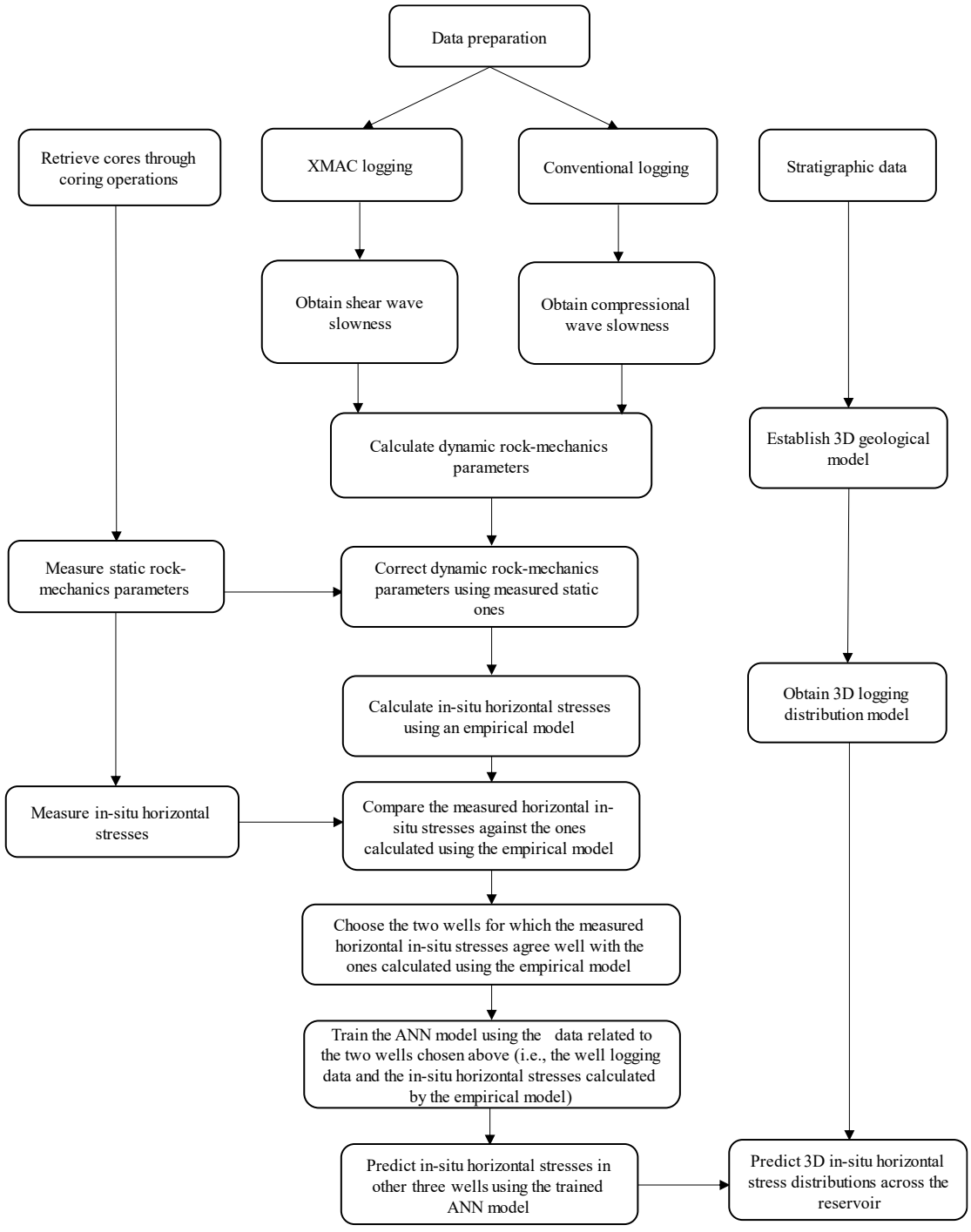

Figure 6 Flowchart of the workflow that is developed in this study.

3.1 Determination of Rock-Mechanics Parameters

Depending on the method used to obtain the rock-mechanics parameters (including Young's modulus and Poisson's ratio), the rock-mechanics parameters can be divided into

two types, namely static rock-mechanics parameters and dynamic rock-mechanics parameters. The static rock-mechanics parameters in this thesis are the ones obtained by using uniaxial or triaxial loading tests in the laboratory, while the dynamic parameters are the ones obtained by the interpretation of the well logging data (Yale et al., 1994).

The dynamic rock-mechanics parameters, i.e., Young's modulus (E) and Poisson's ratio (v), can be calculated based on the following equations (Zhang et al., 2006):

$$E = \frac{\rho}{\Delta t_s{}^2} \frac{3\Delta t_s{}^2 - 4\Delta t_p{}^2}{\Delta t_s{}^2 - \Delta t_p{}^2} \tag{1}$$

$$v = \frac{1}{2} \frac{\Delta t_s{}^2 - 2\Delta t_p{}^2}{\Delta t_s{}^2 - \Delta t_p{}^2} \tag{2}$$

where Δt_p and Δt_s are the compressional wave slowness and the shear wave slowness, which are obtained from XMAC logging data and sonic logging data, respectively; ρ is the bulk density obtained by density logging. Since the dynamic rock-mechanics parameters obtained by logging data may deviate from the real ones, we need to covert these dynamic parameters to the static ones according to the measured Young's modulus and Poisson's ratio. **Figure 7** shows the relationship between the dynamic Poisson's ratio obtained based on the logging data and the static experimental data, while **Figure 8** shows the relationship between the dynamic Young's modulus obtained based on the logging data and the static experimental data. It can be seen from Figures 7 and 8 that the static rock-mechanics parameters correlate well with the dynamic ones. Based on the results shown in Figures 7 and 8, we obtain a linear relation between the dynamic and static Poisson's

ratios, as well as a linear relation between the dynamic and static Young's modulus, as shown below:

$$y = 2.5219x - 0.3421 \quad (3)$$

$$y = 0.3868x + 11.825 \quad (4)$$

where x is the dynamic Poisson's ratio or the dynamic Young's modulus; y is the static Poisson's ratio or the static Young's modulus. Note that the coefficients of determination, R^2, of the above two regressions are 0.8293 and 0.8082, respectively. This indicates that the corrections as per Equations (3) and (4) are with good accuracy.

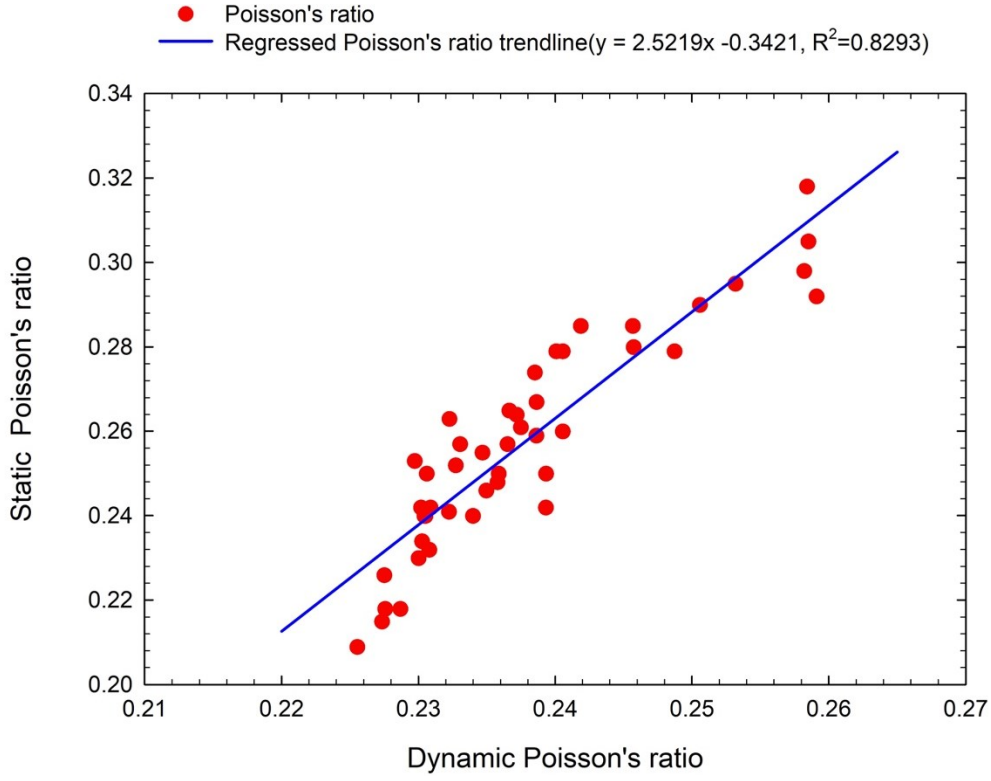

Figure 7 Relationship between the dynamic Poisson's ratio obtained based on the logging data and the static experimental data.

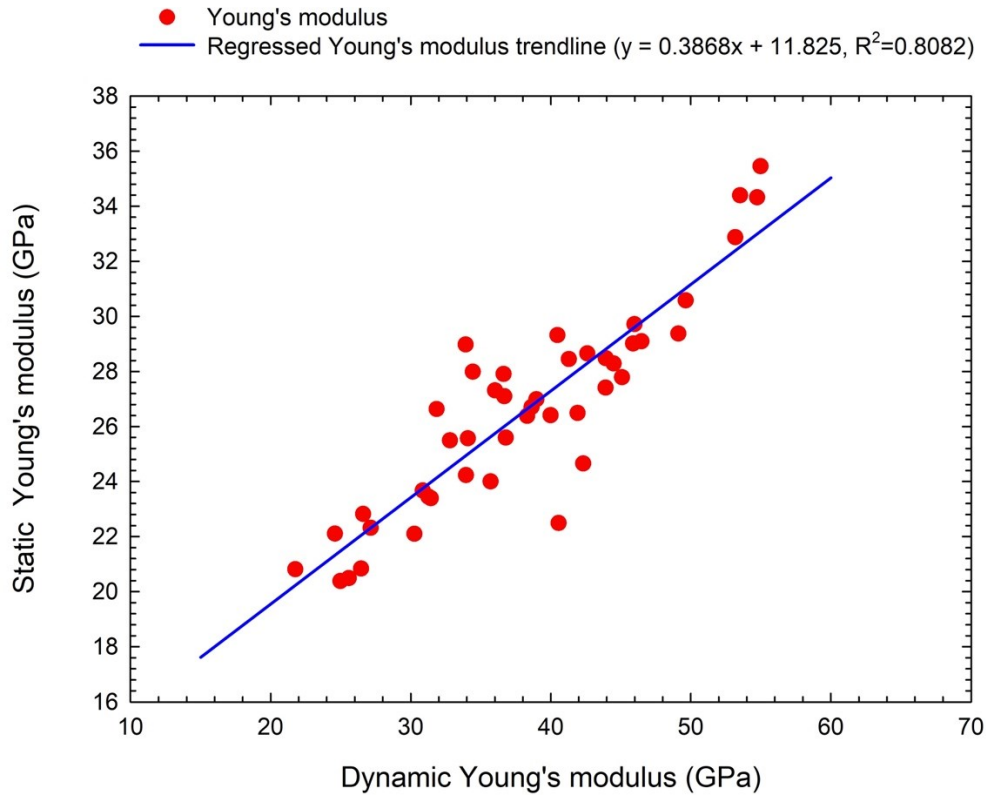

Figure 8 Relationship between the dynamic Young's modulus obtained based on the logging data and the static experimental data.

3.2 Prediction of In-situ Stresses

3.2.1 Conventional Method for Calculating In-situ Stresses

Vertical stress is caused by the weight of the overlying formations. It can be calculated by using density logging data. The expression of the vertical stress is given by (Eaton, 1975):

$$S_v = \int_0^h \rho(h)\, g \cdot dh \tag{5}$$

where S_v is the vertical stress magnitude; h is the depth; $\rho(h)$ is the density of the formation obtained from density logging; g is the acceleration of gravity.

The in-situ horizontal stresses are mainly caused by the overlying strata pressure, tectonic stress, creep of the rock formation, and rise of pore pressure. In this thesis, the pore

elasticity equation proposed by Thiercelin and Plumb (1994) is used to calculate the maximum and minimum horizontal in-situ stresses in the study area (Thiercelin and Plumb, 1994):

$$SH_{min} = \frac{\nu}{1-\nu}(S_v - \alpha P) + \frac{E\varepsilon_h}{1-\nu^2} + \frac{\nu E\varepsilon_H}{1-\nu^2} + \alpha P \quad (6)$$

$$SH_{max} = \frac{\nu}{1-\nu}(S_v - \alpha P) + \frac{E\varepsilon_H}{1-\nu^2} + \frac{\nu E\varepsilon_h}{1-\nu^2} + \alpha P \quad (7)$$

where SH_{max} is the maximum in-situ horizontal stress magnitude; SH_{min} is the minimum in-situ horizontal stress magnitude; α is the Biot coefficient; P is the pore pressure that can be obtained from the drilling records; ε_h and ε_H are the strain constants in the direction of the minimum and maximum horizontal stresses, respectively. ε_h and ε_H are mainly used to characterize the additional in-situ horizontal stresses due to tectonic stresses. It should be noted that α, ε_h, and ε_H are optimized as 1, 0.000205, and 0.000726 in this study area, respectively.

3.2.2 ANN Model

3.2.2.1 Establishment of ANN Model

BP neural network is one of the most widely used neural network models. Its main structure consists of an input layer, a hidden layer, and an output layer. The core of this method is to use the gradient descent method to adjusting and the connection weights and thresholds of the network (Abbas et al., 2020). **Figure 9** shows the basic structure of the BP neural network (Ahmed et al., 2018). We assume that there are n inputs and m outputs

in a neural network, and s neurons in the hidden layer.

The output of the hidden layer, the output of the ANN model, and the error function can be calculated by (Ding et al., 2011):

$$b_j = f_1\left(\sum_{i=1}^{n} w_{ij}x_i - \theta_j\right) (i = 1,2,\dots,n; j = 1,2,\dots,s) \quad (8)$$

$$y_k = f_2\left(\sum_{j=1}^{n} w_{jk}b_j - \theta_k\right) (j = 1,2,\dots,s; k = 1,2,\dots,m) \quad (9)$$

$$e = \sum_{k=1}^{m}(t_k - y_k)^2 \quad (10)$$

where b_j is the *j*th output of the hidden layer; y_k is the *k*th output of the neural network; t_k is the actual output value (real value); e is the squared error between calculated outputs and real values; x_i is the *i*th input value; θ_k is the *k*th threshold of the output layer; θ_j is the *j*th threshold of the hidden layer; f_1 is the transfer function of the hidden layer; f_2 is the transfer function of the output layer; w_{ij} is the connection weight between the *i*th input and the *j*th neuron; w_{jk} is the connection weight between the *j*th neuron and the *k*th output. In the training process, the neurons in the hidden layer and the output layer first receive the inputs from the forward layer. Then all the inputs are summed up with different weights. Next, the new outputs are calculated through an activation function. Based on the calculated error between the predicted outputs and the actual outputs, the model uses the back-propagation method to update the weights and thresholds in each neuron (Ahmed et al., 2018; Alzate et al., 2014). The updating is stopped until the calculated error is acceptable (Ahmed et al., 2018; Alzate et al., 2014).

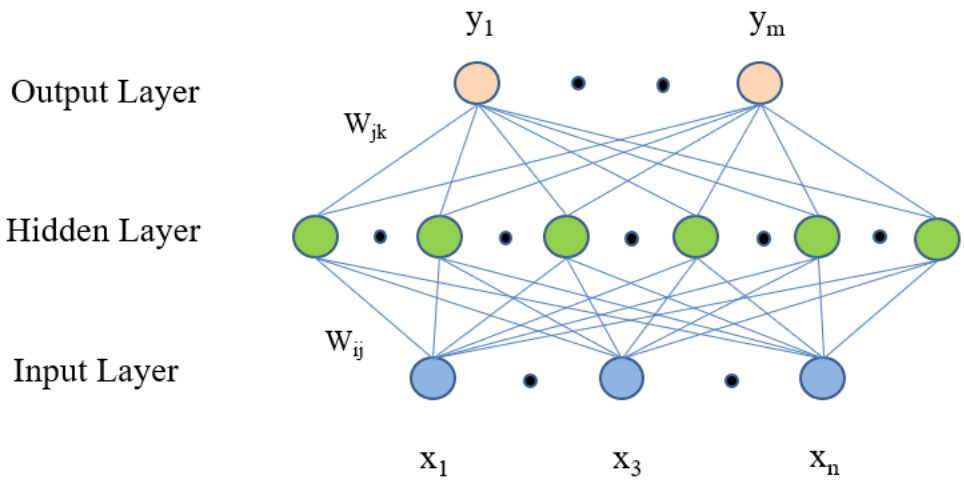

Figure 9 The basic structure of the BP neural network (Ahmed et al., 2018).

(1) The selection of input parameters

Although XMAC logging (DTS) data is available among all the five wells in this study area, it could be missing in the other areas due to its high cost. Besides, due to the weight of overlying formations, depth is also a significant factor that effects the magnitudes of the in-situ stresses. As a result, aiming to make the ANN model more inclusive, we select depth (DEP), sonic logging (AC), neutron logging (CNL), density logging (DEN), and gamma-ray logging (GR) as the input parameters to carry out the correlation analysis in this study area.

(2) Construction of the neural network structure

ANN model structure affects the prediction accuracy and the computational efficiency. If the number of neurons is too small, the accuracy of the model is not satisfactory. But if the number of neurons is too large, it will not only increase the training time but also increase

the learning error. This thesis uses Matlab to build a 4-layer BP neural network model, including one input layer, two hidden layers, and one output layer. The BP neural network structure is illustrated in **Figure 10**. The input layer has five inputs (i.e., DEP, AC, CNL, DEN, and GR). The two hidden layers have 10 and 8 neurons, respectively. The output layer has two outputs (i.e., SH_{min} and SH_{max}).

(3) Preparation of the training samples

The experimental in-situ stress data are normally quite limited. To address this issue, we propose a hybrid method, which combines neural networks and conventional rock mechanics, to achieve better predictions of in-situ horizontal stresses. First, the in-situ stress magnitudes of the five wells are calculated using the conventional rock-mechanics method (i.e., Equations 1-7). The results show that the calculated in-situ stress magnitudes of well Y1 and well Y3 agree well with the measured ones. Next, we apply the empirical model as represented by Equations 1-7 to obtain the continuous profiles of SH_{min} and SH_{max}. At last, the well logging data (DEP, AC, CNL, DEN, and GR), together with the continuously calculated profiles of SH_{min} and SH_{max}, are used as the training data for building the ANN model.

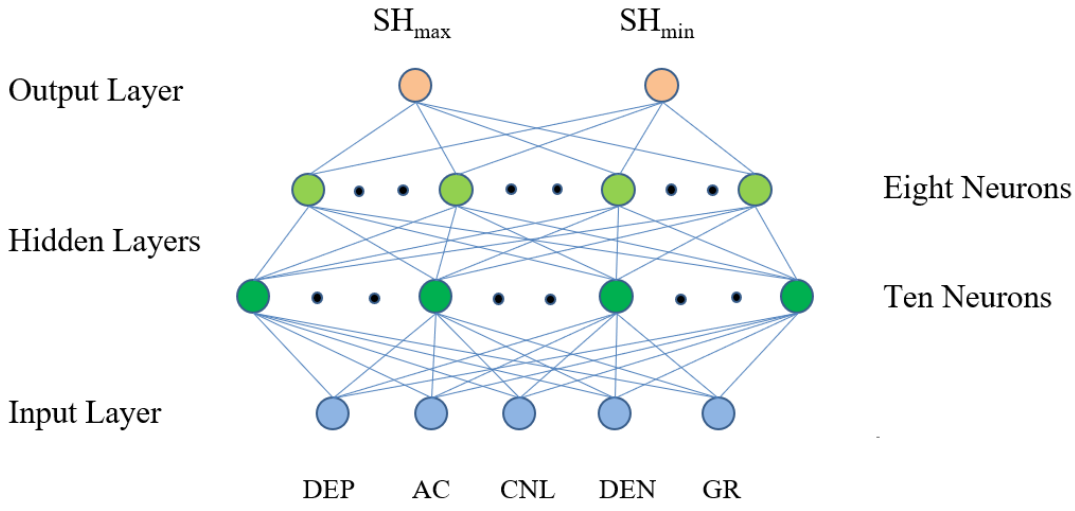

Figure 10 Optimized structure of the ANN model established in this study.

3.2.2.2 Training Process

The training process of the ANN model includes setting input and output values, designing the hidden layers and the neurons of each layer, and setting the learning rate and allowable error. The samples are divided into three parts randomly (train set: 70%, validation set: 15%, and test set: 15%). The Levenberg-Marquardt back-propagation algorithm in Matlab is selected for learning and training the ANN model. The activation function is a nonlinear Sigmoid function, and the learning and training rate is 0.1. Mean squared error is used as the error standard of the training progress, which is set as $10e^{-5}$ (i.e., the goal value). **Figure 11** shows the evolution of the squared error during the training process. The training process is completed automatically at the tenth epoch, leading to a mean squared error of $7.8518e^{-6}$.

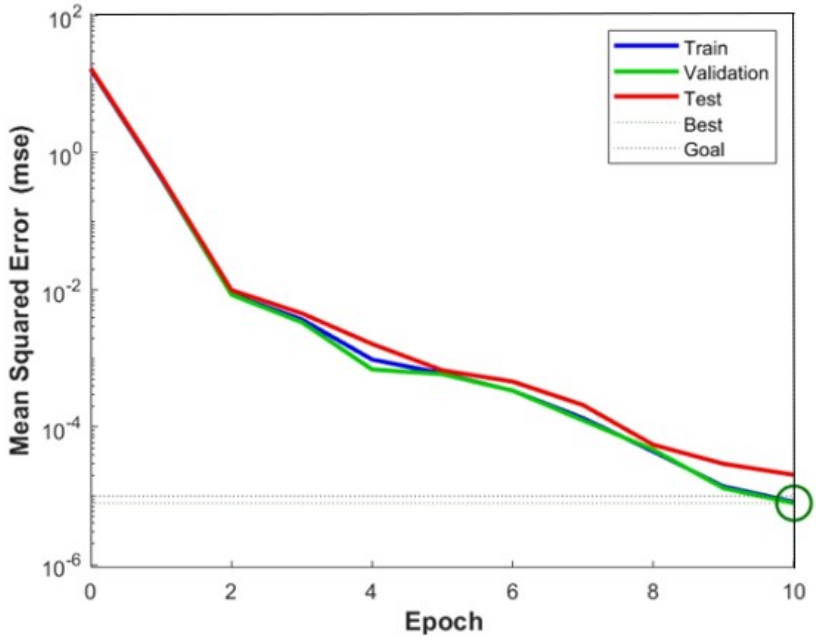

Figure 11 Evolution of the mean squared error during the training process.

3.3 Prediction of 3D In-situ Stress

3.3.1 Establishment of 3D Geological Model

In this study, the software Petrel is adopted to establish the 3D geological model for the study area of Longmaxi formation in southwest China. Firstly, the lithology of different formations, the depths of different formations, and the structural plane data are input into Petrel. Then the fault model and the layer model are established in sequence. Based on the lithology of different formations and the trend of structural surface data, an interpolation model is established. As the geological stratification is known, the interpolation of each layer is carried out according to the sedimentation laws. Finally, a 3D geological model of the study area is obtained and shown in **Figure 12**.

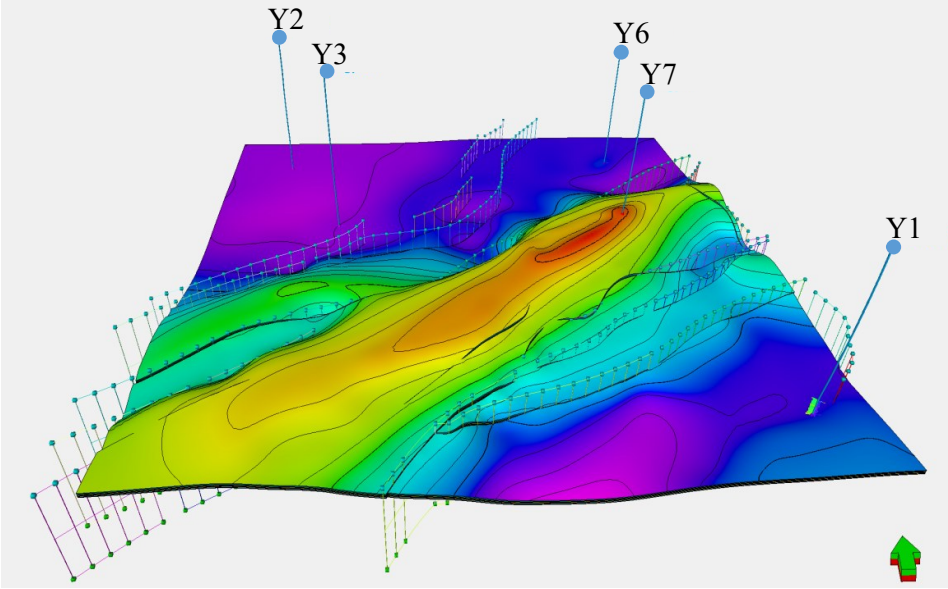

Figure 12 The 3D geological model established in this study for the study area of Longmaxi formation in southwest China.

3.3.2 Establishment of Spatial Distribution Models of Logging Parameters

Figure 13 presents the spatial distribution models of the AC, CNL, DEN, GR, and DEP parameters that are established based on the interpolation of the logging data of the five wells. The Kriging interpolation algorithm is adopted for the spatial interpolations. Based on the obtained spatial distributions of logging parameters, the established ANN model can predict the magnitudes of horizontal in-situ maximum and minimum stresses in the study area.

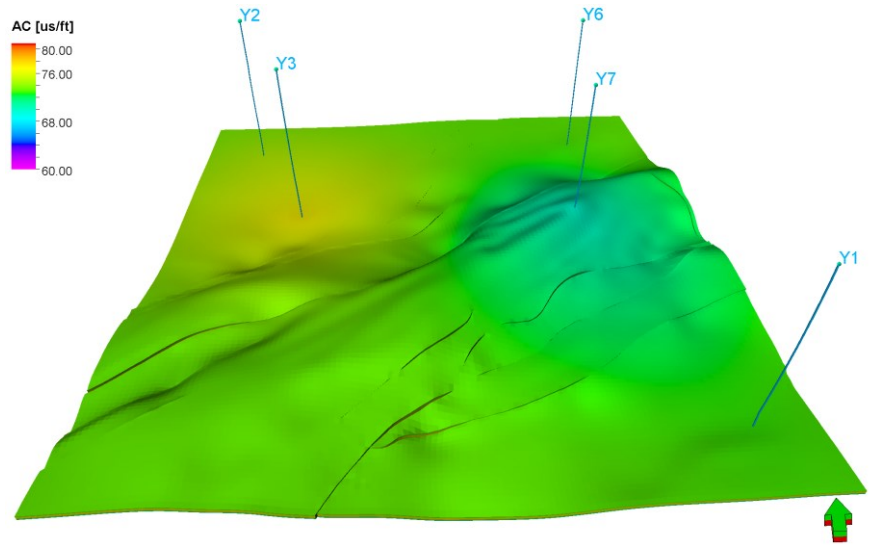
AC [us/ft]
80.00
76.00
68.00
60.00
Y2
Y3
Y6
Y7
Y1

(a)

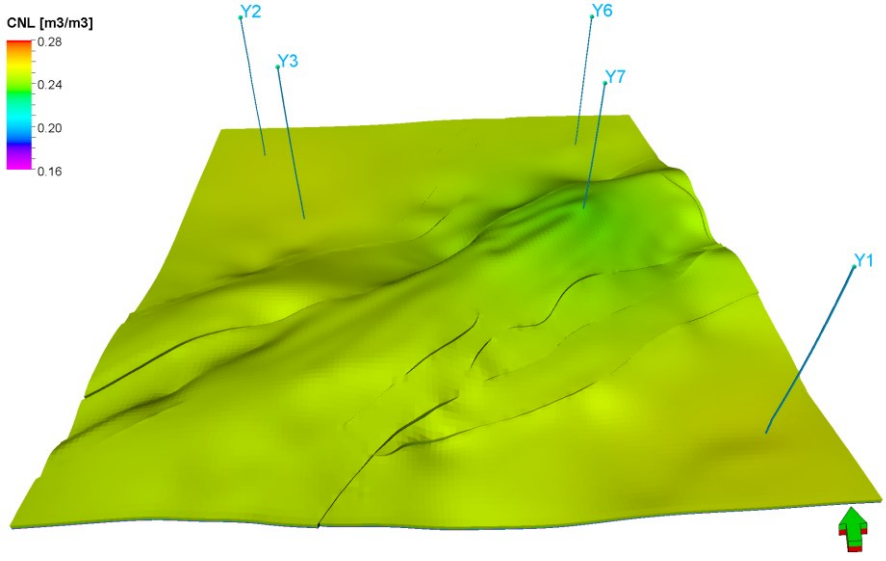
CNL [m3/m3]
0.28
0.24
0.20
0.16
Y2
Y3
Y6
Y7
Y1

(b)

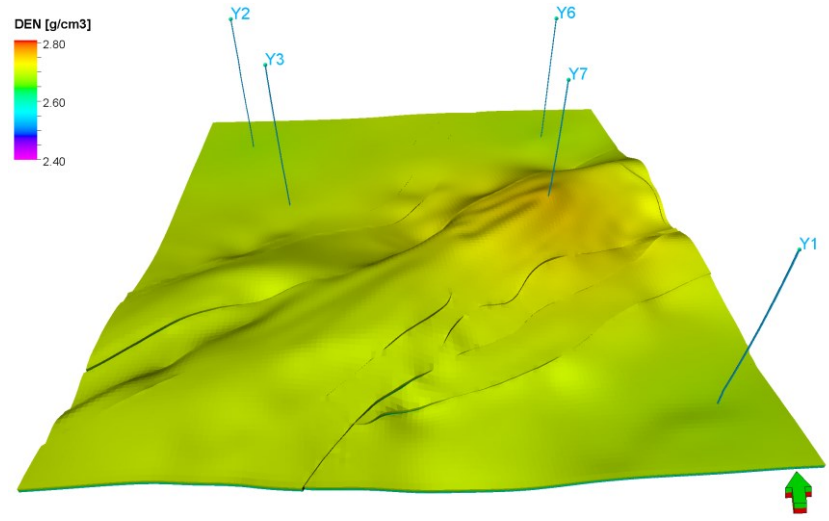
DEN [g/cm3]
2.80
2.60
2.40
Y2
Y3
Y6
Y7
Y1

(c)

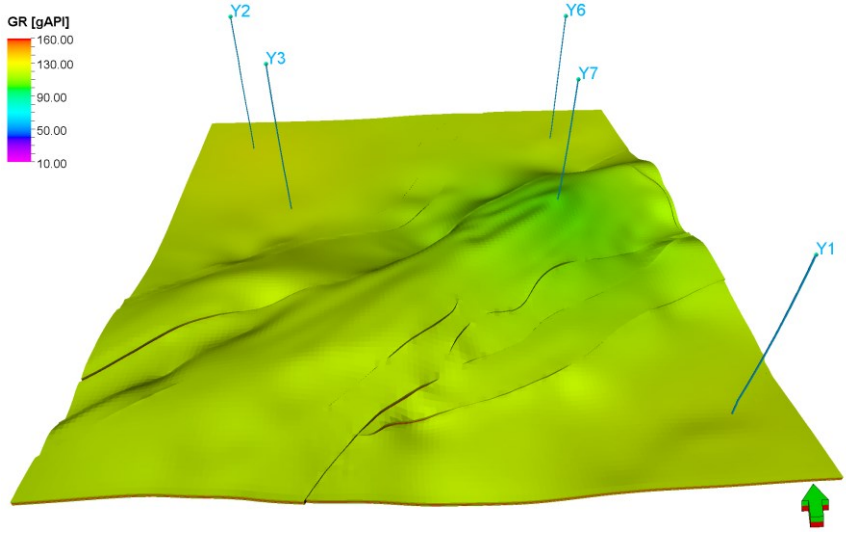
GR [gAPI]
160.00
130.00
90.00
50.00
10.00
Y2
Y3
Y6
Y7
Y1

(d)

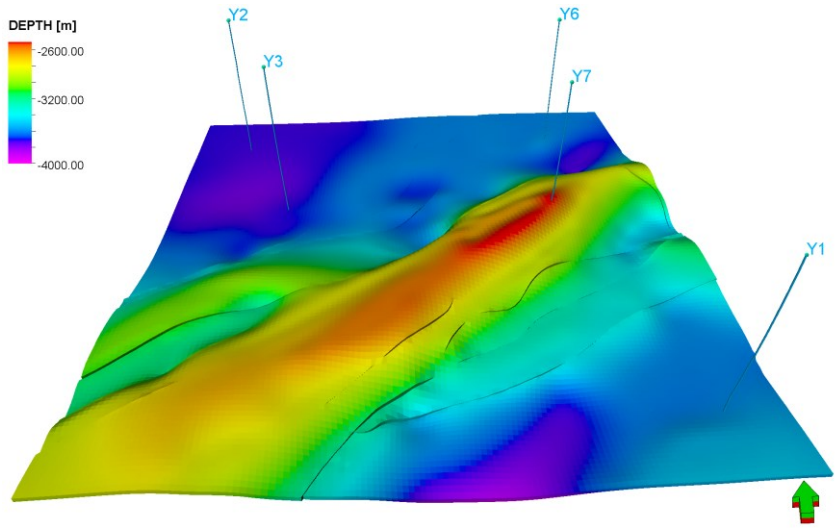

(e)

Figure 13 The spatial distribution models of different logging parameters: (a) AC; (b) CNL; (c) DEN; (d) GR; (e) DEP.

References

Abbas, A., Alsaba, M., Al, D., Dahm, H., Alhumairi, M. (2020). Determination of Minimum Horizontal Stress Magnitudes from Conventional Well Logging Data Using Artificial Neural Network. Paper ARMA 20–1495 presented at the 54th US Rock Mechanics/Geomechanics Symposium held in Golden, Colorado, USA.

Alzate, G., Agudelo, A. (2014). Generating Synthetic Well Logs by Artificial Neural Networks (ANN) Using MISO-ARMAX Model in Cupiagua Field. Paper SPE-169388-MS presented at the SPE Latin American and Caribbean Petroleum Engineering Conference held in Maracaibo, Venezuela.

Ahmed, E.B., Ahmed, A., Ahmed, E.M. (2018). PVT Property Correlations Selection and

Estimation. Gulf Professional Publishing.

Biot, M. (1941). General Theory of Three-Dimensional Consolidation. Journal of Applied Physics, 12, 155-164.

Ding, S., Su, C., Yu, J. (2011). An Optimizing BP Neural Network Algorithm Based on Genetic Algorithm. Artificial Intelligence Review, 36, 153-162.

Eaton, B. (1972) Graphical Method Predicts Geopressure Worldwide. World Oil, 182, 51-56.

Eaton, B. (1975). The Equation for Geo-pressure Prediction from Well Logs. Paper SPE-5544-MS presented at the Fall Meeting of the Society of Petroleum Engineers of AIME, Dallas, Texas.

Geertsma, J. (1957). A Remark on the Analogy Between Thermo-elasticity and Elasticity of Saturated Porous Media. Journal of the Mechanics and Physics of Solids, 6(1), 13-16.

Lin, Z., Sun, Z., Hu, H., Xu, K., Lei, C. (2020). Pore Pressure Distributional Characterization of Shale Gas Reservoir in WR Block of Sichuan Basin. Progress in Geophysics, 36(5), 2045-2052.

Rickman, R., Mullen, M., Petre, E., Grieser, B., Kundert, D., (2008). A Practical Use of Shale Petrophysics for Stimulation Design Optimization: All Shale Plays are Not

Clones of the Barnett Shale. Paper SPE 115258 presented at Annual Technical Conference and Exhibition. Denver, Colorado, USA, 21–24 September.

Shan, Y., Liu, W. (2000). Experimental Study on Dynamic and Static Mechanics Parameters of Rocks Under Formation Conditions. Journal of Chengdu University of Technology, 27(3), 249-254.

Thiercelin, M.J., Plumb, R.A. (1994). Core-Based Prediction of Lithologic Stress Contrasts in East Texas Formations. SPE Formation Evaluation, 9 (04), 251-258.

Xu, G. Zhong, G., Xie, B., Huang, T. (2014). Petrophysical Experimental-based Logging Evaluation Method of Shale Brittleness. Natural Gas Industry, 34(12), 38-45.

Yale, D., Corp, M., Jamieson, W. (1994). Static and Dynamic Rock Mechanical Properties in the Hugoton and Panoma Fields, Kansas. SPE, 27939.

Yin, X., Ma, N., Ma, Z., Zong, Z. (2018). Review of In-situ Stress Prediction Technology. Geophysical Prospecting for Petroleum, 57(4), 488-504.

Zhang, D., Ranjith, P., Perera, M. (2016). The Brittleness Indices Used in Rock Mechanics and Their Application in Shale Hydraulic Fracturing: A Review. Journal of Petroleum Science and Engineering, 143, 158-170.

CHAPTER 4 RESULTS AND DISCUSSION

This chapter shows the calculation results of the rock-mechanics parameters (including Young's modulus and Poisson's ratio). Then based on the rock-mechanics parameters, the maximum horizontal in-situ stress magnitudes and minimum horizontal in-situ stress magnitudes for individual wells are determined by the newly developed neural network. Finally, by combining the geological model and the developed ANN model, we further obtain the 3D in-situ stress distribution maps in the study area.

4.1 Rock-Mechanics Parameters

Figures 14-18 show the profiles of the rock-mechanics parameters in the study area obtained using the method presented in Chapter 3.1. We can see that the corrected rock mechanics parameters (static curves) fit better with the experimental data than the original ones (dynamic curves).

Figures 19 and **20** show the plane distribution diagrams of Poisson's ratio and Young's modulus, respectively. In Figure 19, the Poisson's ratio ranges from 0.22 to 0.31. The blue area, where the Y6 well is located, has the lowest Poisson's ratio. The central anticline area, where the Y7 well is located, has the highest Poisson's ratio (red area). In summary, the Poisson's ratio gradually decreases from the central anticline area to the surroundings. The plane distribution of Young's modulus is similar to that of Poisson's ratio (see **Figure 20**).

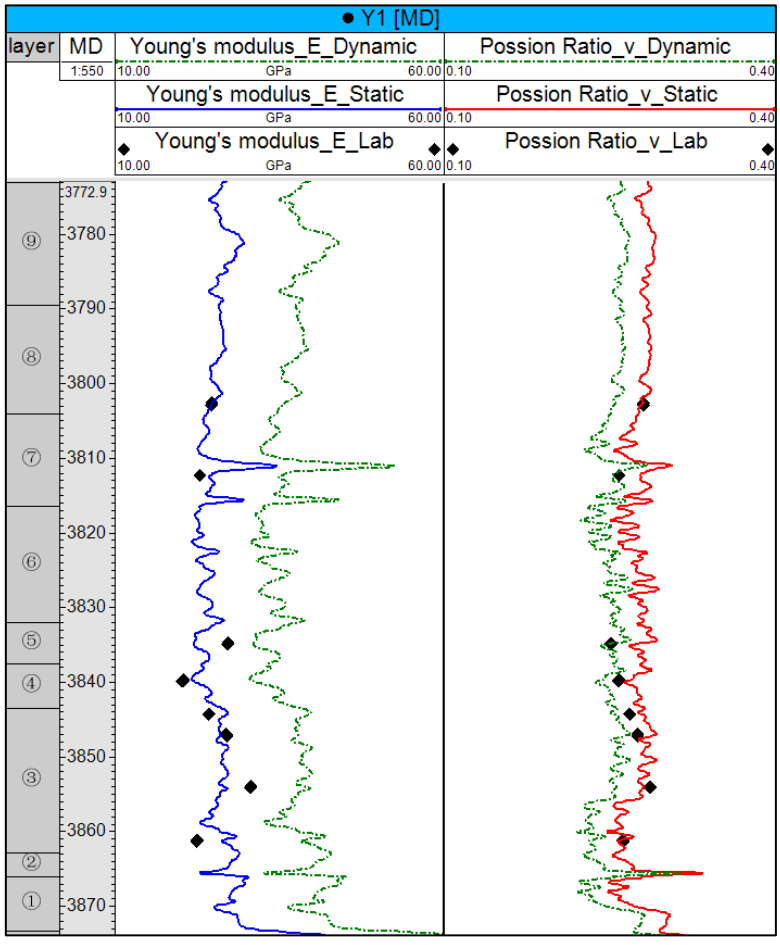

Figure 14 Profiles of Young's modulus and Poisson's ratio for well Y1.

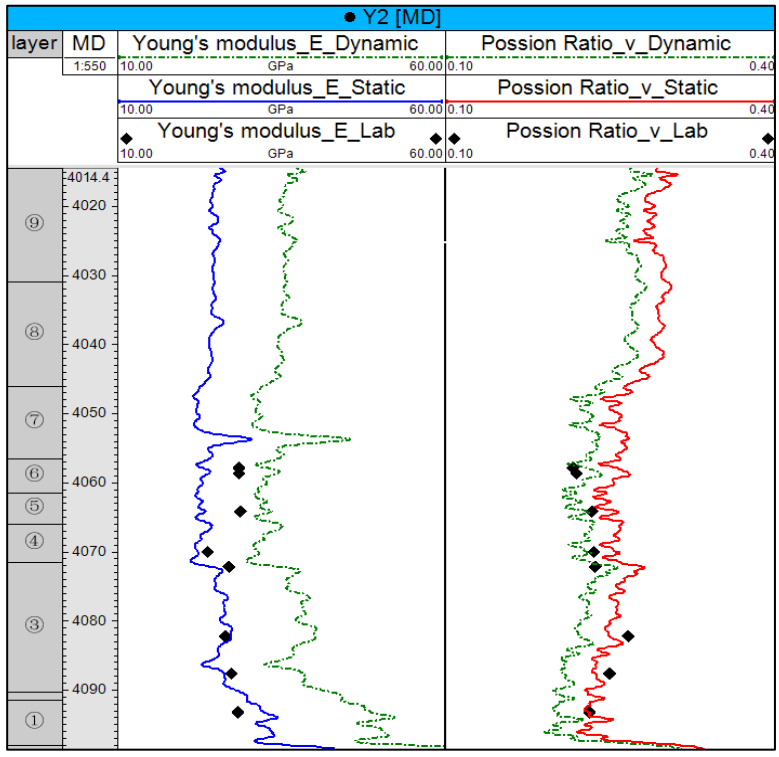

Figure 15 Profiles of Young's modulus and Poisson's ratio for well Y2.

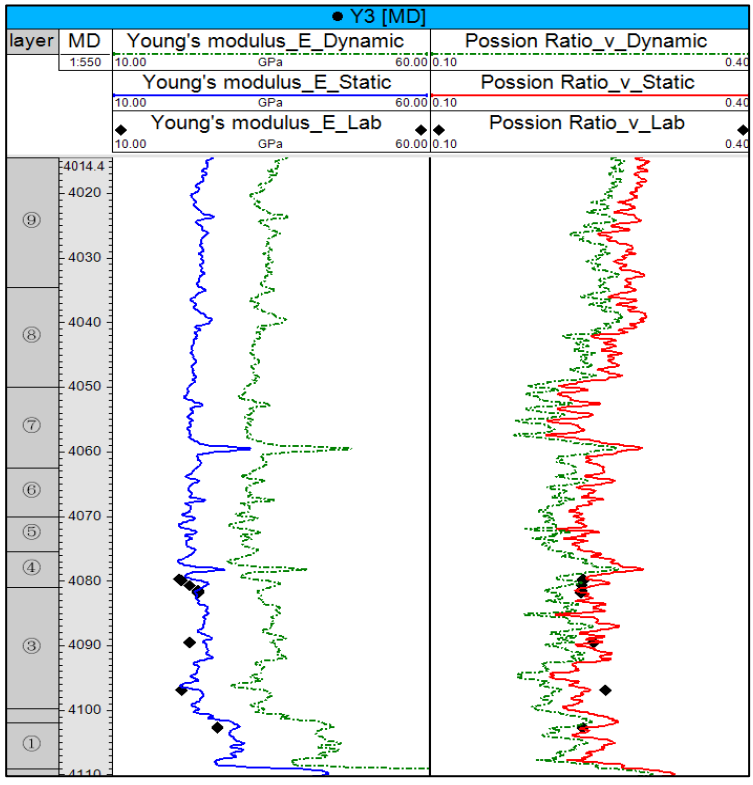

Figure 16 Profiles of Young's modulus and Poisson's ratio for well Y3.

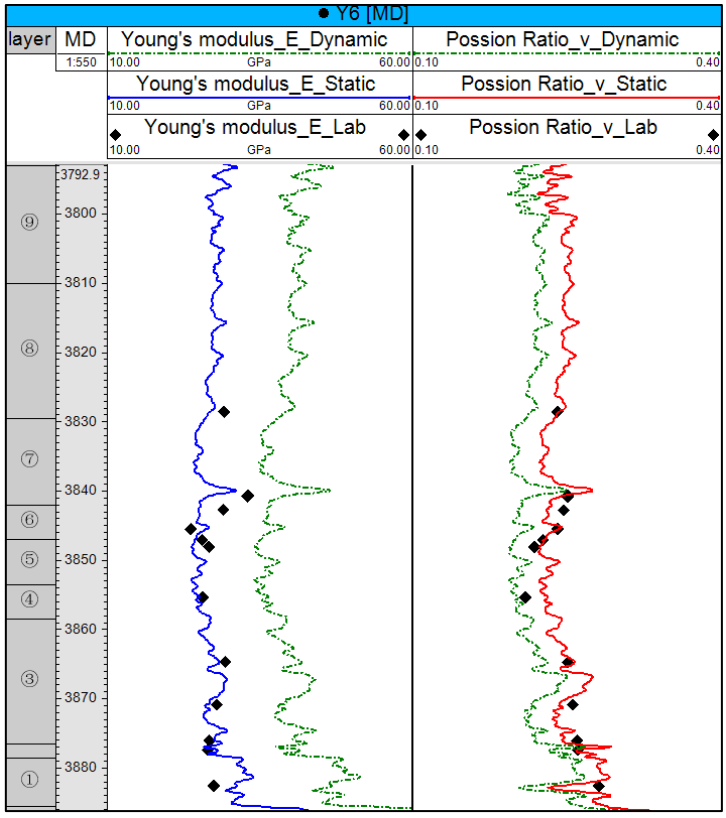

Figure 17 Profiles of Young's modulus and Poisson's ratio for well Y6.

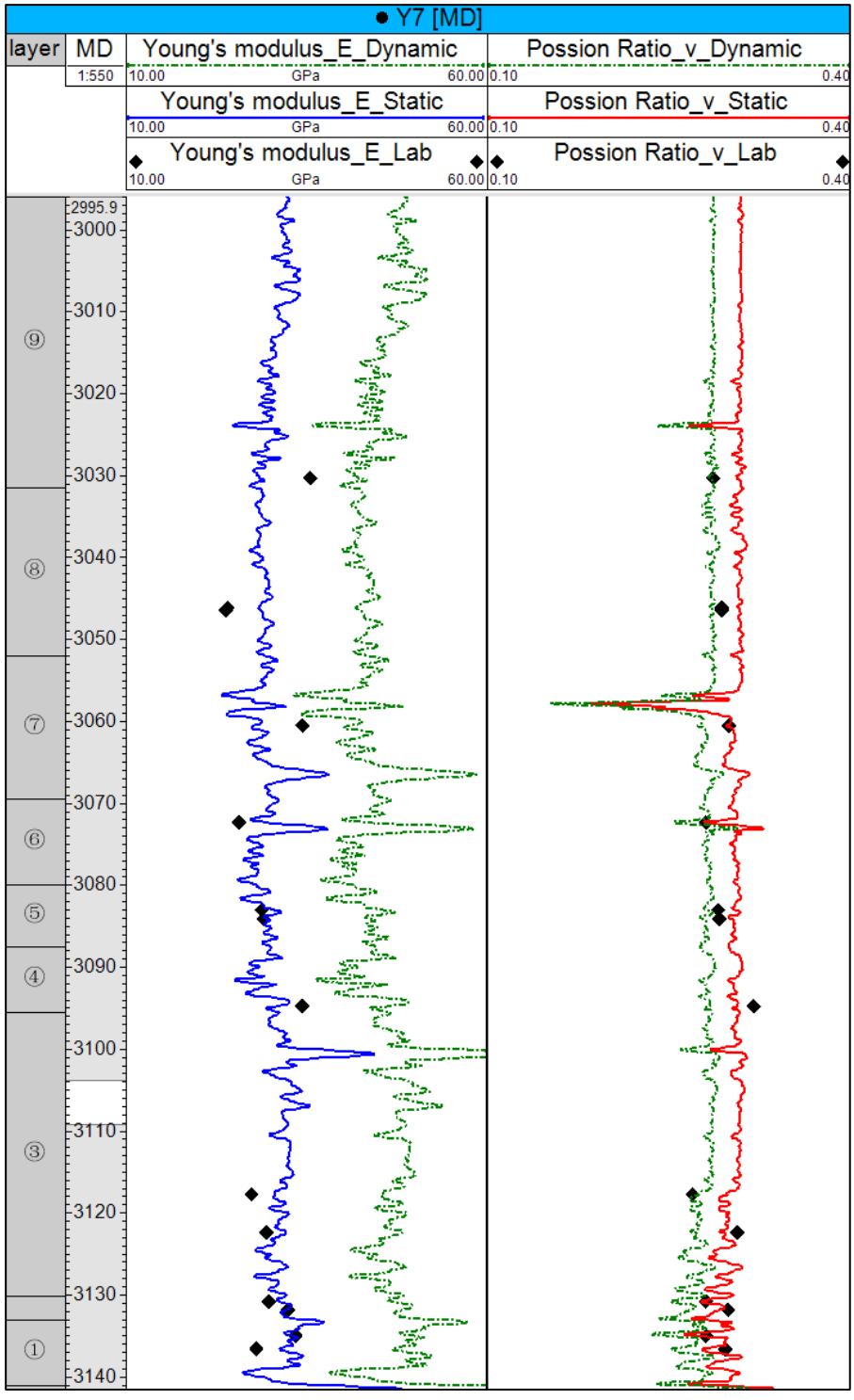

Figure 18 Profiles of Young's modulus and Poisson's ratio for well Y7.

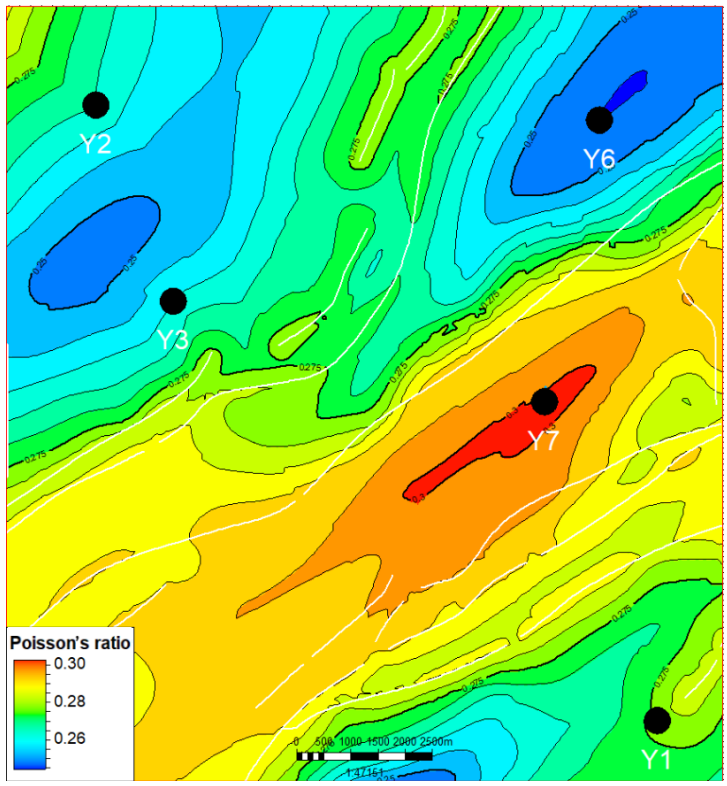

Figure 19 Plane distribution of Poisson's ratio in the study area.

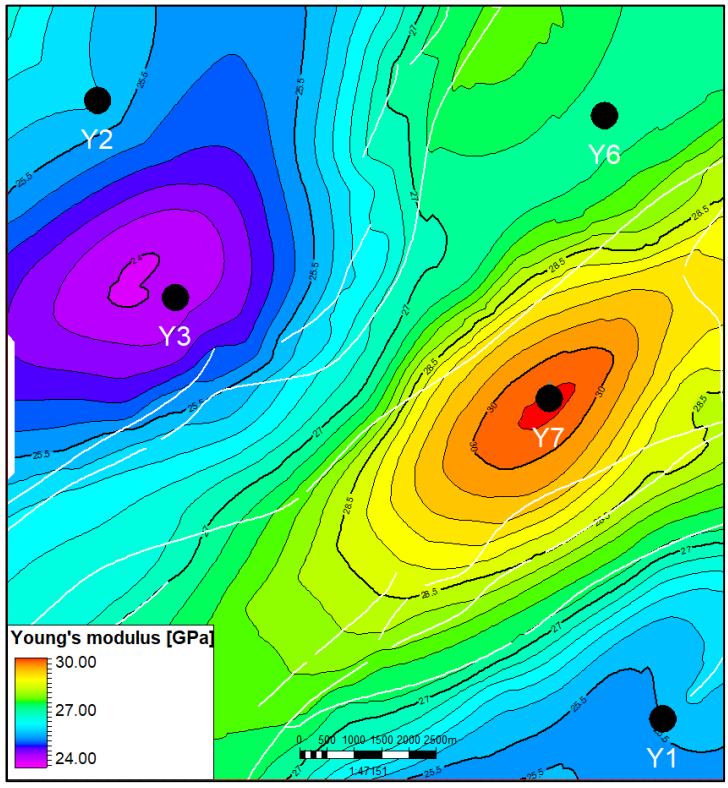

Figure 20 Plane distribution map of Young's modulus in the study area.

4.2 Predictions of In-situ Horizontal Stresses for Single Wells

4.2.1 Conventional Rock-Mechanics Method

Figures 21-25 present the profiles of the in-situ stress magnitudes of the 5 wells based on the conventional methods (Chapter 3.2.1). The calculation and prediction errors used in this thesis are calculated as:

$$MAPE = \frac{100\%}{n}\sum_{i=1}^{n}\left|\frac{(SH_A - SH_E)}{SH_E}\right| \quad (8)$$

where $MAPE$ is the mean absolute percentage error in calculating or predicting the in-situ horizontal stresses; SH_A is the calculated or predicted in-situ horizontal stress magnitude; SH_E is the measured in-situ horizontal stress magnitude; n is the total number of the measured points in a well.

Table 2 summarizes the prediction errors of in-situ maximum and minimum horizontal stress magnitudes based on the conventional methods (Equations 6 and 7). The calculation errors vary from 2.82% to 8.05%, and the average calculation errors for the maximum and minimum horizontal in-situ stress magnitudes are 3.99% and 4.81%.

Table 2 Calculation errors of the in-situ stresses by the conventional rock-mechanics method.

Well number	Depth (m)	SH_{max}, %	SH_{min}, %
Y1	3773-3875	2.82	2.87
Y2	4015-4100	3.29	5.24
Y3	4015-4110	2.04	3.27
Y6	3793-3886	3.75	5.02
Y7	2996-3141	8.05	7.63
Average		3.99	4.81

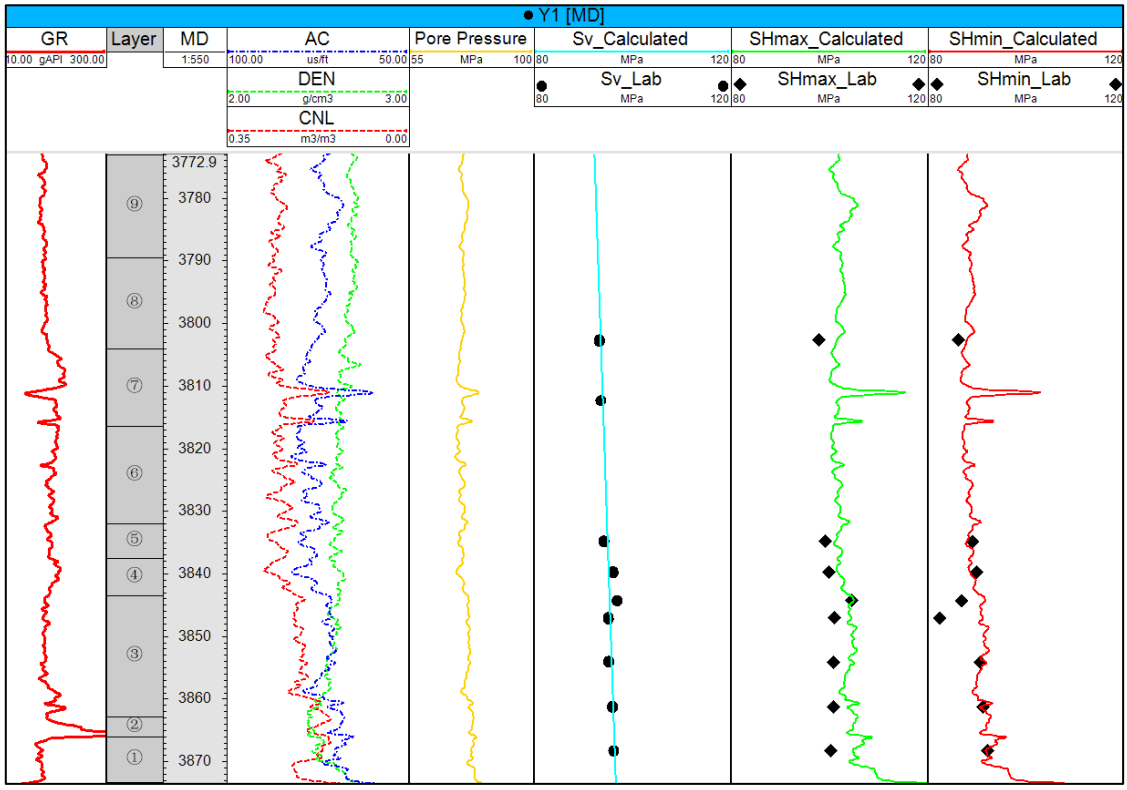

Figure 21 Calculated in-situ stresses of well Y1 based on the conventional rock-mechanics method.

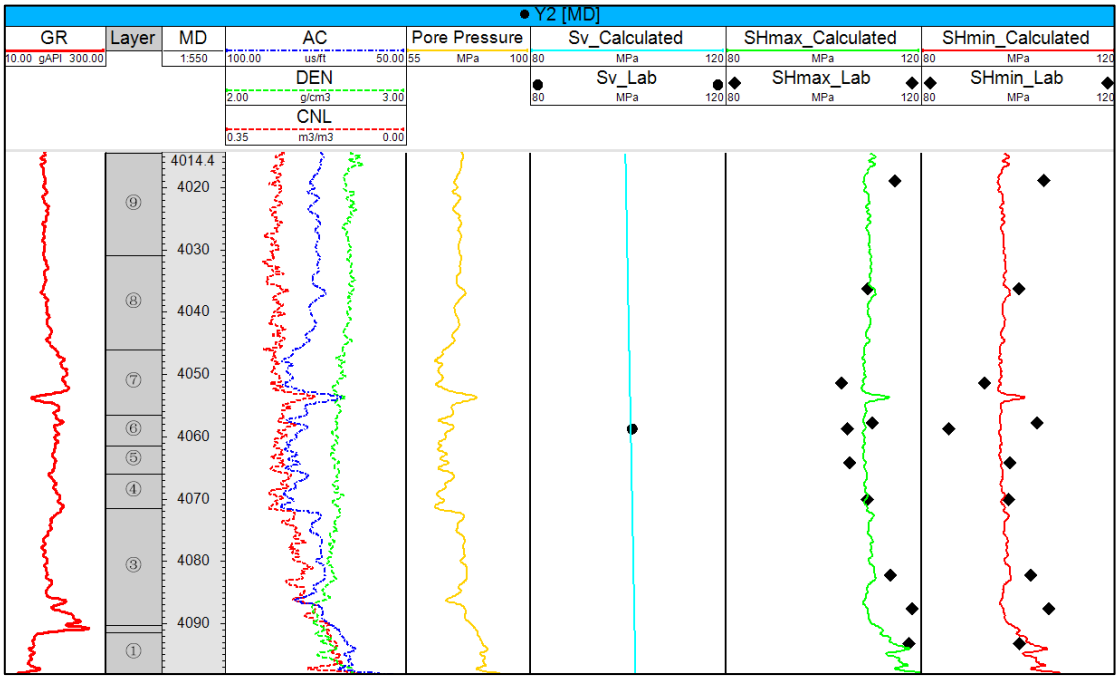

Figure 22 Calculated in-situ stresses of well Y2 based on the conventional rock-mechanics method.

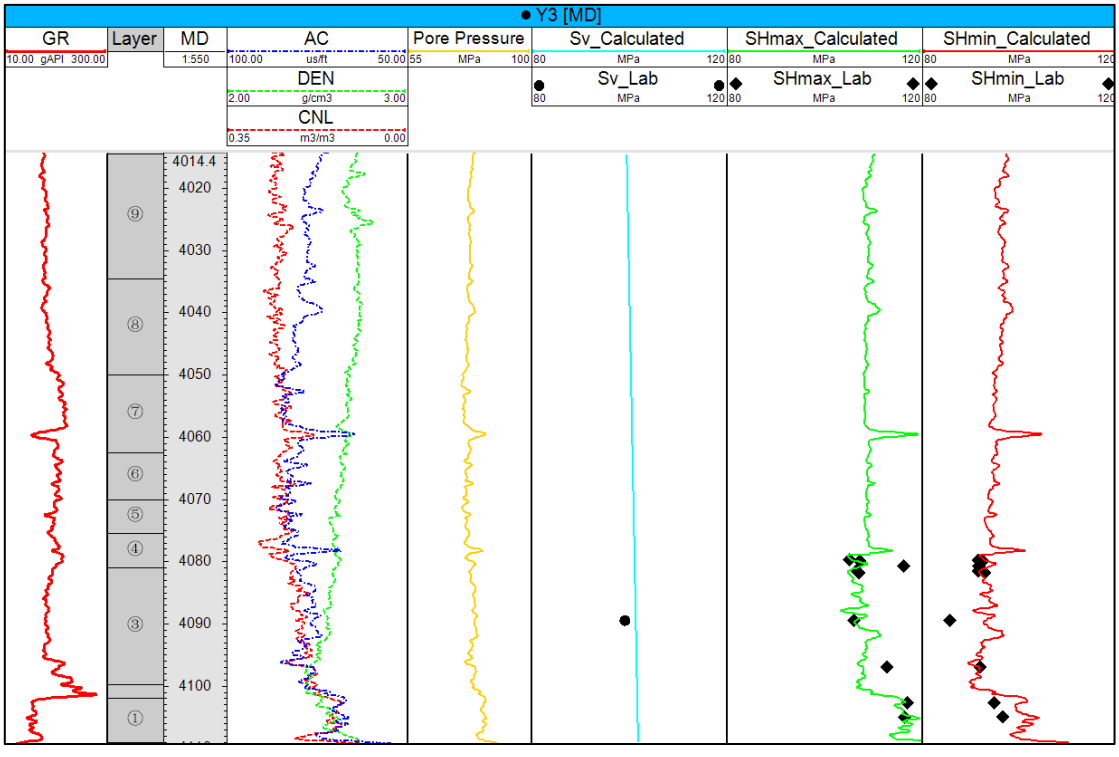

Figure 23 Calculated in-situ stresses of well Y3 based on the conventional rock-mechanics method.

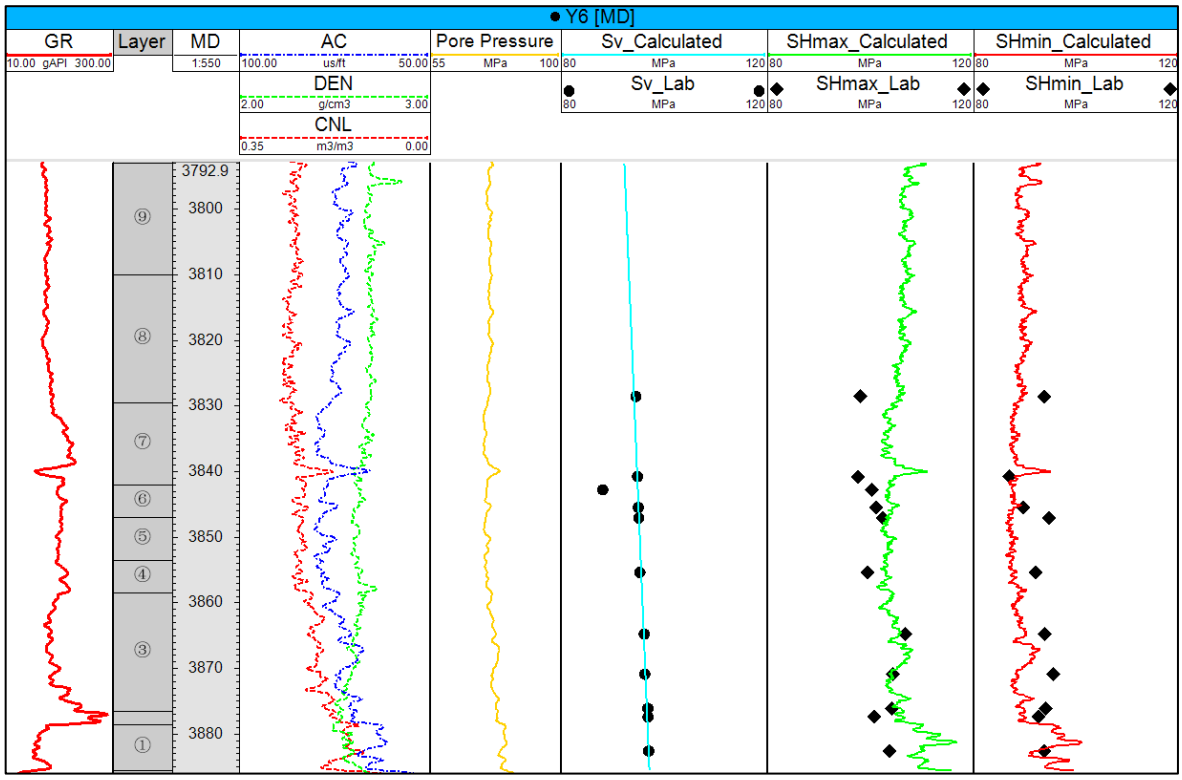

Figure 24 Calculated in-situ stresses of well Y6 based on the conventional rock-mechanics method.

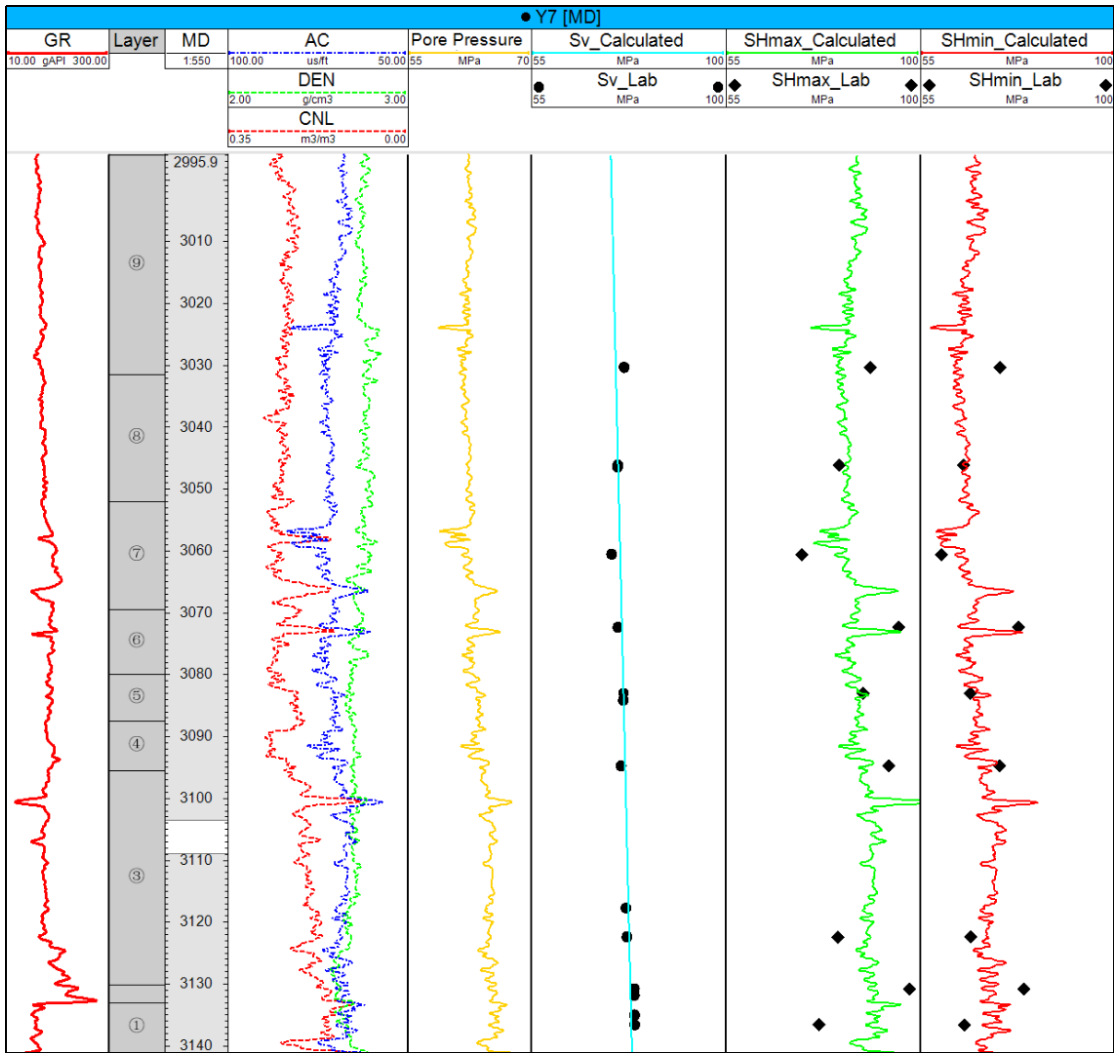

Figure 25 Calculated in-situ stresses of well Y7 based on the conventional rock-mechanics method.

4.2.2 ANN

We employ the newly developed ANN (Chapter 3.2.2) to predict the in-situ maximum and minimum horizontal stresses for Y2, Y6, and Y7 wells. **Figures 26-28** show the predicted magnitudes of the in-situ stresses in the three wells. The *MAPEs* yielded by different models are summarized in **Table 3**. The *MAPEs* in predicting the in-situ maximum and minimum horizontal stresses yielded by the ANN model trained by the newly generated

data are 3.27% and 3.76%. These calculation errors are lower than those yielded by the conventional rock-mechanics method (5.03% and 5.96%). Therefore, the method proposed in this study to generate a large database is reliable, and the ANN model trained with the newly generated data can provide accurate predictions of the in-situ horizontal stresses in this study area.

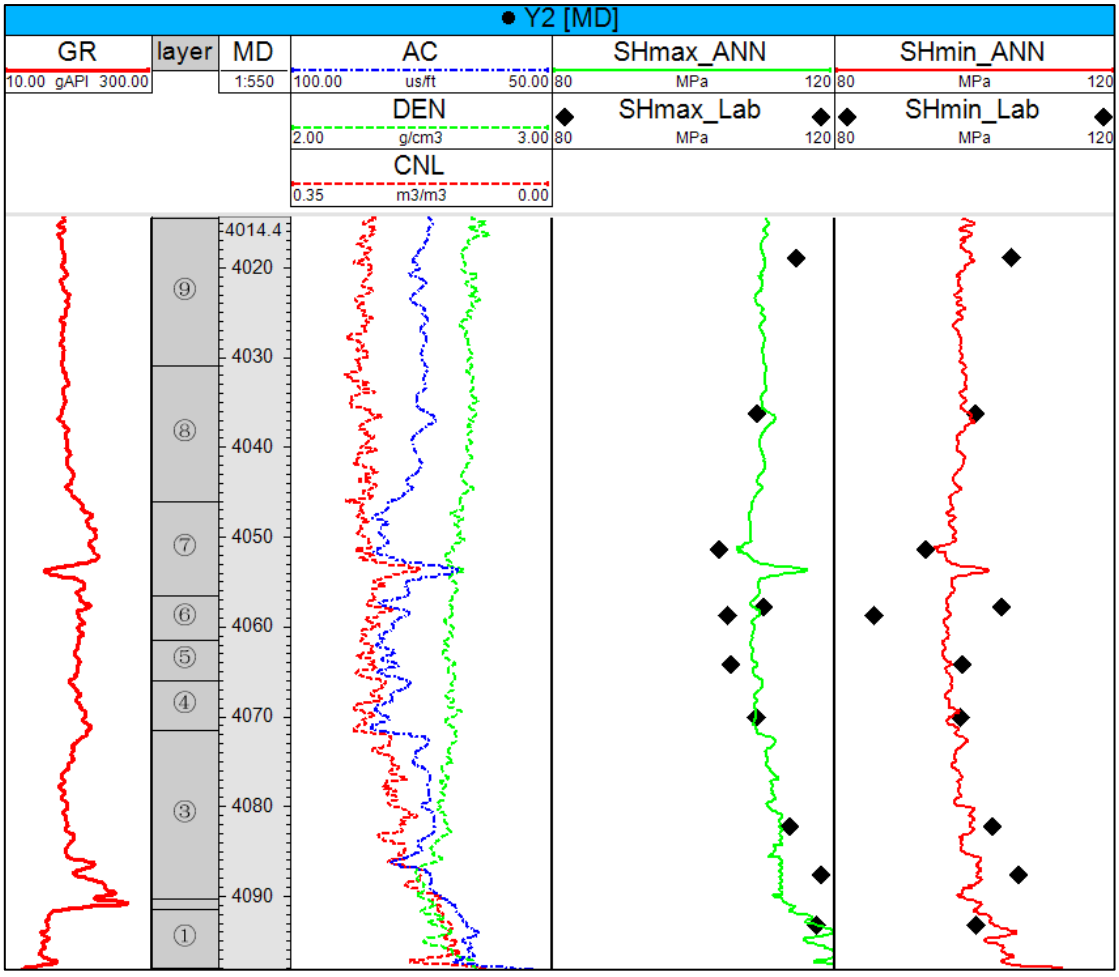

Figure 26 Predicted magnitudes of in-situ horizontal stresses in well Y2 using the ANN model trained by the newly generated training data.

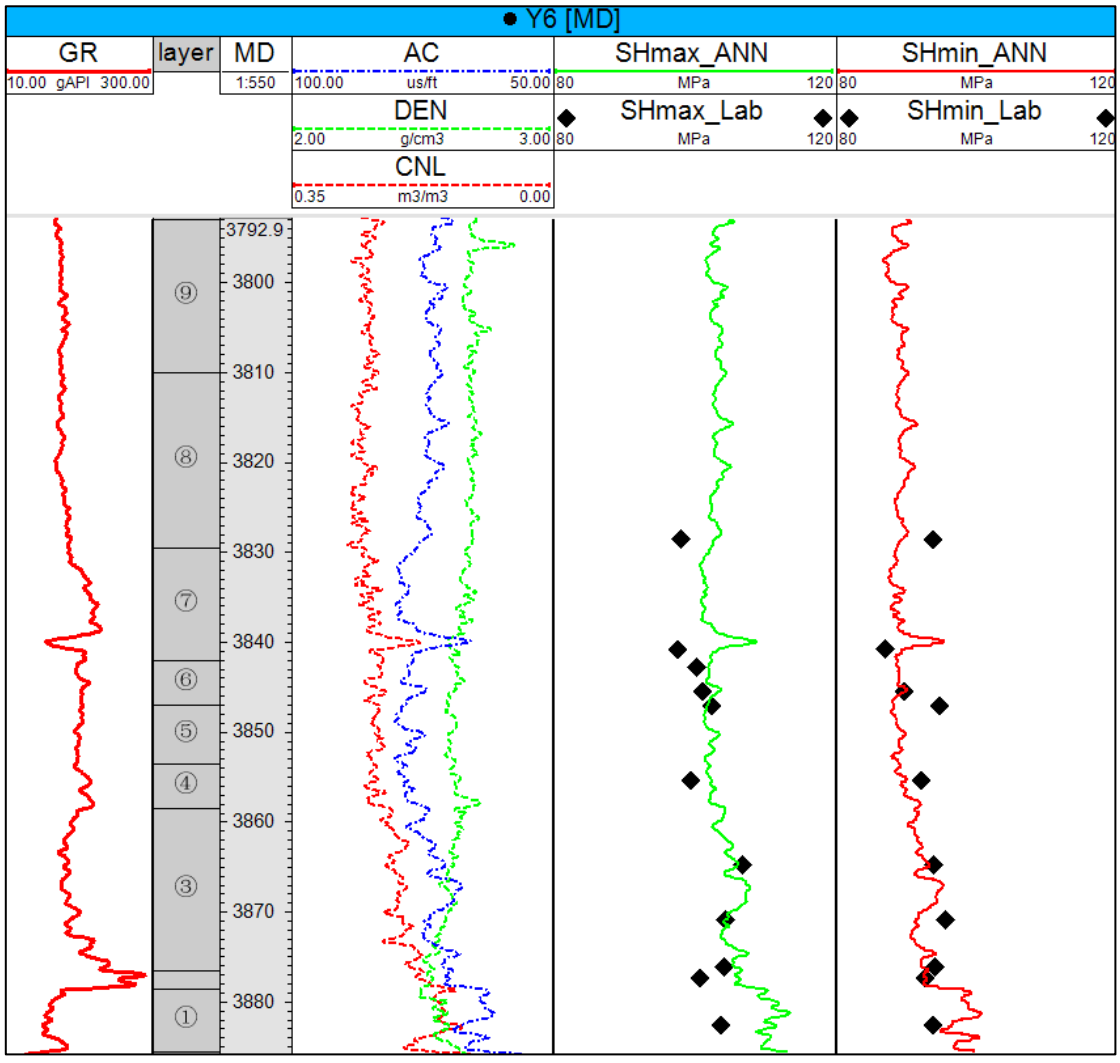

Figure 27 Predicted magnitudes of in-situ horizontal stresses in well Y6 using the ANN model trained by the newly generated training data.

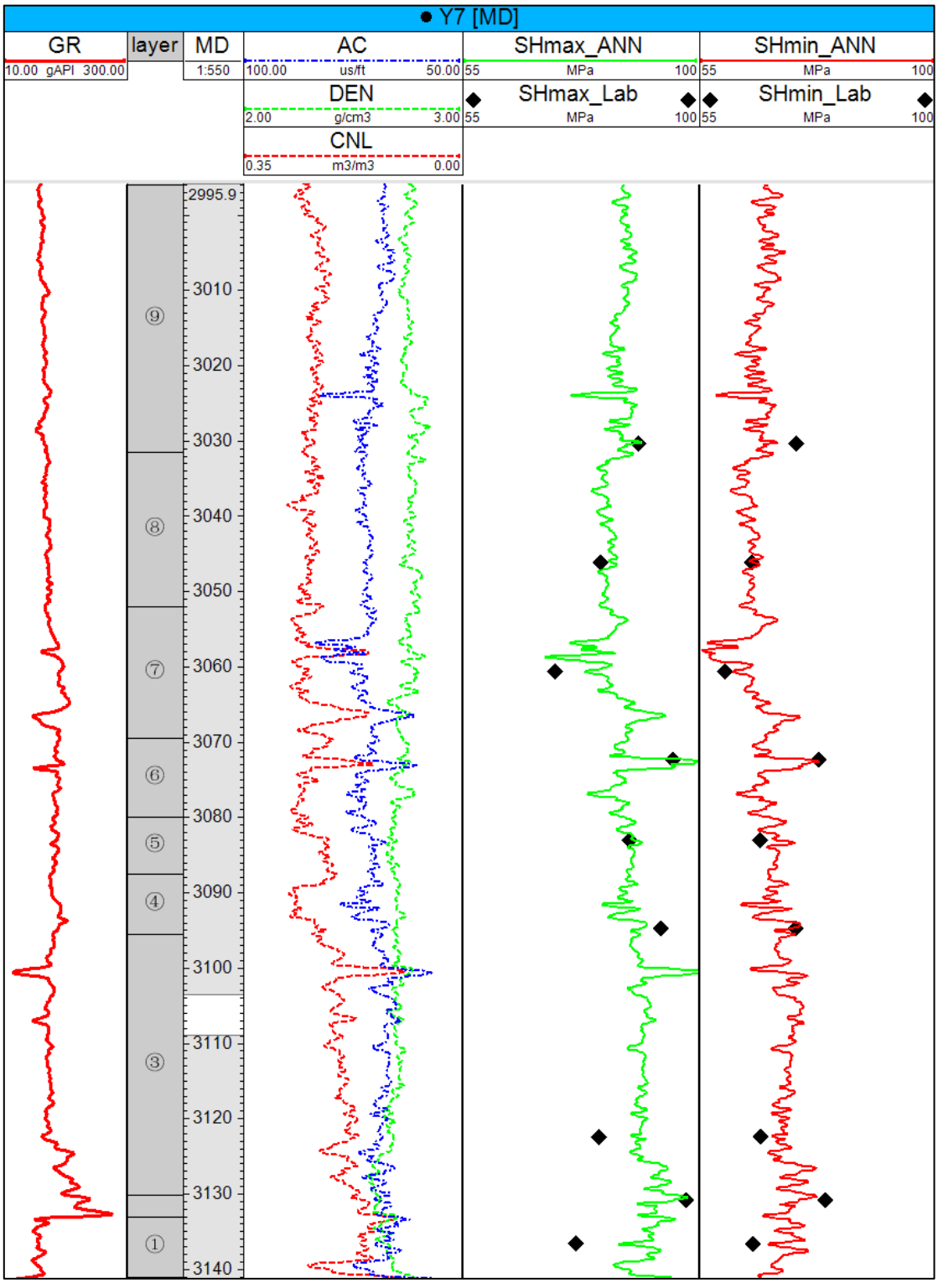

Figure 28 Predicted magnitudes of in-situ horizontal stresses in well Y7 using the ANN model trained by the newly generated training data.

Table 3 MAPEs in predicting the magnitudes of in-situ horizontal stresses yielded by the ANN model trained by the newly generated data, and the conventional rock-mechanics method.

Well number	ANN trained by the newly selected data (%)		Conventional rock-mechanics method (%)	
	SH_{max}	SH_{min}	SH_{max}	SH_{min}
Y2	2.39	4.27	3.29	5.24
Y6	3.07	3.34	3.75	5.02
Y7	4.36	3.68	8.05	7.63
Average	3.27	3.76	5.03	5.96

4.3 Prediction of 3D In-situ Stresses in the Study Area

Figures 29 and **30** show the distributions of the in-situ maximum and minimum horizontal stresses in the study area predicted by the newly developed ANN model, respectively. As shown in **Figure 29**, the in-situ maximum horizontal stress magnitudes in the study area vary from 80.3 MPa to 130 MPa. The in-situ maximum horizontal stress magnitudes in the anticline area are lower than those in the northwest and southeast areas. As seen in **Figure 30**, the minimum horizontal in-situ stress magnitudes in the study area are mainly between 41 MPa to 100 MPa. Similarly, the in-situ minimum horizontal stress magnitudes in the anticline area are also lower than that of other areas. **Figure 31** shows the differences between the maximum and minimum horizontal in-situ stress magnitudes calculated using the developed ANN model in the study area. As shown in **Figure 31**, the stress difference in the study area mainly ranges from 10 MPa to 20 MPa. The stress difference in the

anticline area ranges from 16 MPa to 20 MPa, and the stress difference in the flat area (southeast area and northwest area) ranges from 10 MPa to 16 MPa. These results indicate that the anticline area exhibits larger stress differences and is more suitable for hydraulic fracturing treatments.

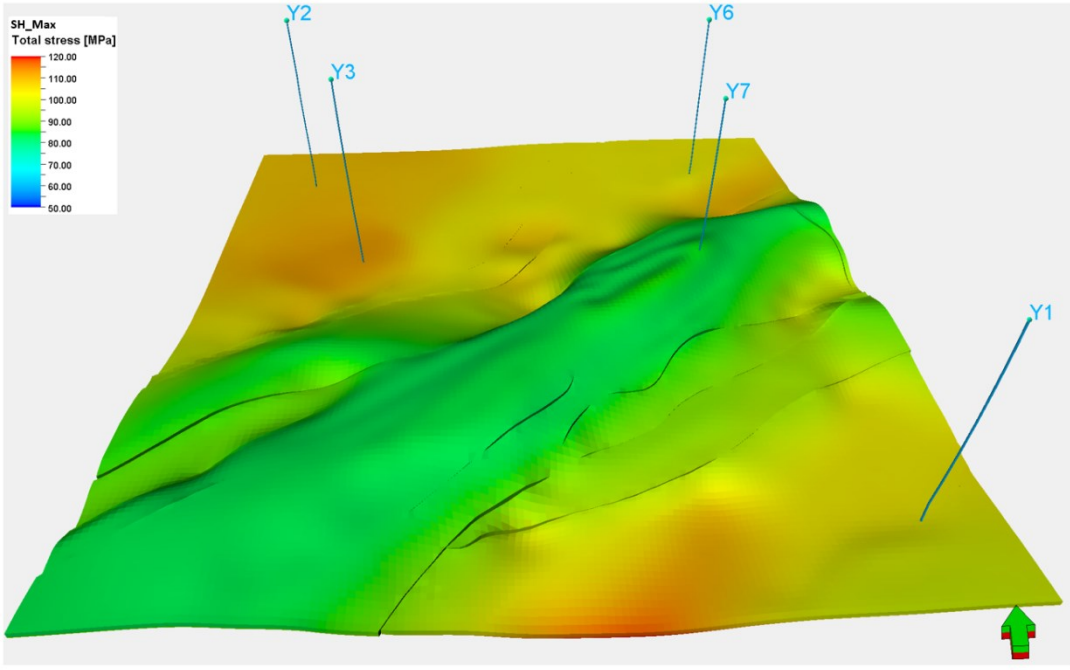

Figure 29 Distribution of in-situ maximum horizontal stress magnitudes yielded by the ANN model developed in this study.

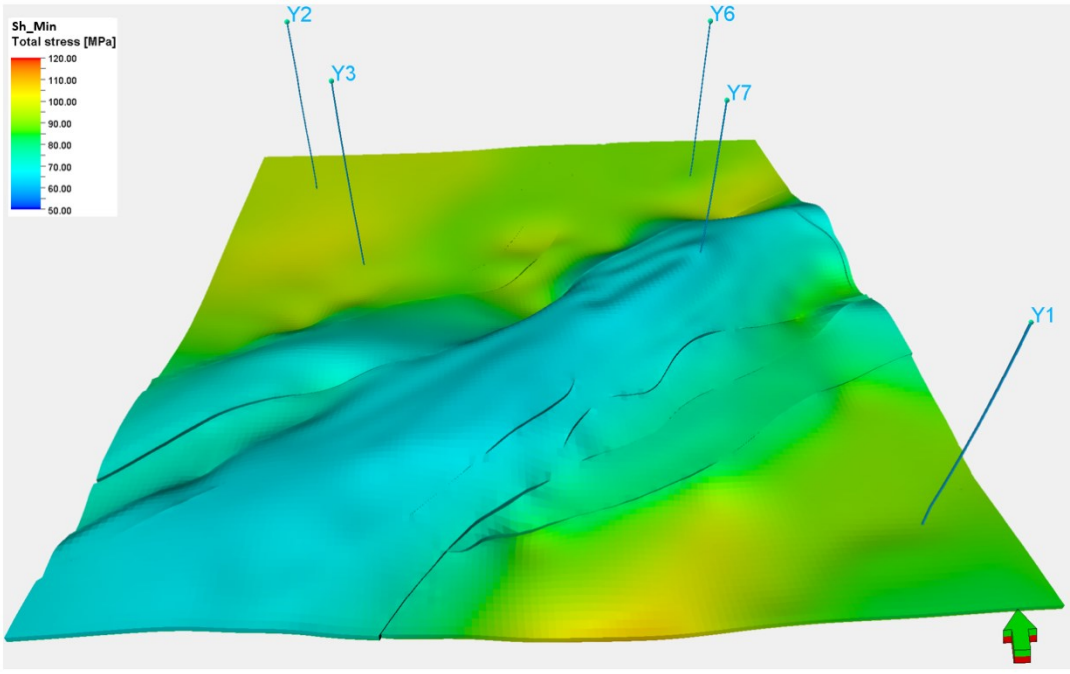

Figure 30 Distribution of in-situ minimum horizontal stress magnitudes yielded by the ANN model developed in this study.

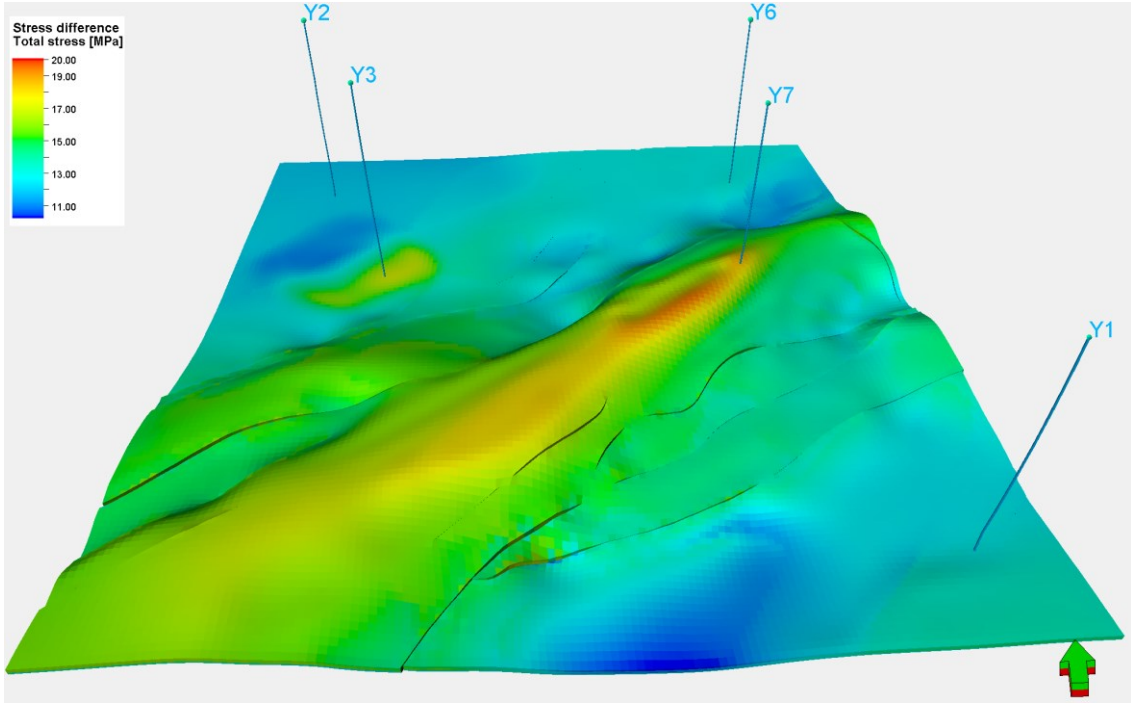

Figure 31 Distribution of the differences between the maximum and minimum horizontal in-situ stress magnitudes calculated using the newly developed ANN model.

CHAPTER 5 CONCLUSIONS AND RECOMMENDATIONS

5.1 Conclusions

In this thesis, a new method for predicting the in-situ horizontal stresses in a shale gas reservoir has been developed based on the artificial intelligence and the conventional rock mechanics. We demonstrate that the newly developed ANN model can be used to more accurately predict the magnitudes of in-situ maximum and minimum horizontal stresses than the conventional methods. Based on the research results, we can form the following conclusions:

- Since the experimental data in this study area are insufficient, this thesis proposes a novel method to generate a large pseudo-experimental training database of in-situ horizontal stresses based on the data in two wells (Well Y1 and Well Y3), for which the calculated in-situ stress magnitudes are in good agreement with the measured in-situ stress magnitudes.
- A 4-layer ANN model is established, which has one input layer, two hidden layers, and one output payer. The input parameters are depth (DEP), sonic logging (AC), neutron logging (CNL), density logging (DEN), and gamma-ray logging (GR). The outputs are the in-situ horizontal stresses. Then the generated large pseudo-experimental training database is used to train the established neural network. Finally, we use this newly trained model to predict the magnitudes of in-situ horizontal stresses in other wells (Well Y2, Y6, and Y7).

- We predict the in-situ horizontal stresses in the other three wells using the trained ANN models and examine the model performance by comparing the calculated ones against the measured ones. It is found that the trained ANN model performs well in predicting the magnitudes of the in-situ horizontal stresses in this study area.
- Finally, a series of 3D in-situ horizontal stress magnitude distribution maps of the study area have been plotted by the newly developed neural network coupled with a geological model. Such 3D distribution maps will be highly useful for guiding the drilling and hydraulic fracturing operations in this study area.

5.2 Recommendations

The hybrid approach developed in this study is proven to be a reliable approach in a small reservoir. Future studies should be conducted to see whether such approach can also be valid in larger-size reservoirs. Furthermore, the logging data applied in this thesis are from 5 wells in which the lithology is shale. Future studies can examine if this approach of combining ANN and conventional rock mechanics can be extended to predict the in-situ stress magnitudes for the conventional reservoirs, such as carbonate and sandstone reservoirs.

BIBLIOGRAPHY

Abbas, A., Alsaba, M., Al, D., Dahm, H., Alhumairi, M. (2020). Determination of Minimum Horizontal Stress Magnitudes from Conventional Well Logging Data Using Artificial Neural Network. Paper ARMA 20–1495 presented at the 54th US Rock Mechanics/Geomechanics Symposium held in Golden, Colorado, USA.

Alzate, G., Agudelo, A. (2014). Generating Synthetic Well Logs by Artificial Neural Networks (ANN) Using MISO-ARMAX Model in Cupiagua Field. Paper SPE-169388-MS presented at the SPE Latin American and Caribbean Petroleum Engineering Conference held in Maracaibo, Venezuela.

Ahmed, E.B., Ahmed, A., Ahmed, E.M. (2018). PVT Property Correlations Selection and Estimation. Gulf Professional Publishing.

Biot, M. (1941). General Theory of Three-Dimensional Consolidation. Journal of Applied Physics, 12, 155-164.

Ding, S., Su, C., Yu, J. (2011). An Optimizing BP Neural Network Algorithm Based on Genetic Algorithm. Artificial Intelligence Review, 36, 153-162.

Eaton, B. (1972). Graphical Method Predicts Geopressure Worldwide. World Oil, 182, 51-56.

Eaton, B. (1975). The Equation for Geo-pressure Prediction from Well Logs. Paper SPE-

5544-MS presented at the Fall Meeting of the Society of Petroleum Engineers of AIME, Dallas, Texas.

Geertsma, J. (1957). A Remark on the Analogy Between Thermo-elasticity and Elasticity of Saturated Porous Media. Journal of the Mechanics and Physics of Solids, 6(1), 13-16.

Haimson, B., Fairhurst, C. (1969). In-situ Stress Determination at Great Depth by Means of Hydraulic Fracturing. Paper ARMA-69-0559 presented at the 11th U.S. Symposium on Rock Mechanics (USRMS), Berkeley, California.

Jenkins, A., Fathi, E, Belyadi, F. (2017). Stress Field Behavior Induced by Hydraulic Fracture in Shale Reservoirs: A Practical View on Cluster Spacing. Journal of Natural Gas Science and Engineering, 48(1), 186-196.

Ju, W., Shen, S., Qin, Y., Meng., Wu, C., Shen, Y., Yang, Z., Li, G., Li, C. (2017). In-Situ Stress State in the Linxing Region, Eastern Ordos Basin, China: Implications for Unconventional Gas Exploration and Production. Marine and Petroleum Geology, 86, 66-78.

Lian, Z., Yu, H., Lin, T., Guo, J. (2015). A Study on Casing Deformation Failure During Multistage Hydraulic Fracturing for the Stimulated Reservoir Volume of Horizontal Shale Wells. Journal of Natural Gas Science and Engineering, 23, 538-546.

Lin, W., Kwaśniewski, M., Imamura, T., Matsuki, K. (2006). Determination of Three-Dimensional In-situ Stresses from Anelastic Strain Recovery Measurement of Cores at Great Depth. Tectonophysics, 426(2), 221-238.

Lin, Z., Sun, Z., Hu, H., Xu, K., Lei, C. (2020). Pore Pressure Distributional Characterization of Shale Gas Reservoir in WR Block of Sichuan Basin. Progress in Geophysics, 36(5), 2045-2052.

Matsuki, K., Takeuchi, K. (1993). Three-dimensional In-situ Stress Determination by Anelastic Strain Recovery of a Rock Core. Paper ARMA-93-0637 presented at the 34th U.S. Symposium on Rock Mechanics (USRMS), Madison, Wisconsin.

Neuzil, C.E. (2019). Permeability of Clays and Shales. Annual Review of Earth and Planetary Sciences, 47, 247–73.

Rasouli, V., Pallikathekathil, Z. J., Mawuli, E. (2011). The Influence of Perturbed Stresses Near Faults on Drilling Strategy: A Case Study in Blacktip Field, North Australia. Journal of Petroleum Science and Engineering, 76, 37-50.

Rickman, R., Mullen, M., Petre, E., Grieser, B., Kundert, D. (2008). A Practical Use of Shale Petrophysics for Stimulation Design Optimization: All Shale Plays are Not Clones of the Barnett Shale. Paper SPE-115258 presented at Annual Technical Conference and Exhibition. Denver, Colorado, USA, 21–24 September.

Seto, M., Nag, D.K., Vutukuri, V.S. (1999). In-Situ Rock Stress Measurement from Rock Cores Using the Acoustic Emission Method and Deformation Rate Analysis. Geotechnical and Geological Engineering, 17, 241-266.

Shan, Y., Liu, W. (2000). Experimental Study on Dynamic and Static Mechanics Parameters of Rocks Under Formation Conditions. Journal of Chengdu University of Technology, 27(3), 249-254.

Thiercelin, M.J., Plumb, R.A. (1994). Core-Based Prediction of Lithologic Stress Contrasts in East Texas Formations. SPE Formation Evaluation, 9 (04), 251-258.

Xu, G. Zhong, G., Xie, B., Huang, T. (2014). Petrophysical Experimental-based Logging Evaluation Method of Shale Brittleness. Natural Gas Industry, 34(12), 38-45.

Yale, D., Corp, M., Jamieson, W. (1994). Static and Dynamic Rock Mechanical Properties in the Hugoton and Panoma Fields, Kansas. SPE, 27939.

Yin, X., Ma, N., Ma, Z., Zong, Z. (2018). Review of In-situ Stress Prediction Technology. Geophysical Prospecting for Petroleum, 57(4), 488-504.

Zhang, D., Ranjith, P., Perera, M. (2016). The Brittleness Indices Used in Rock Mechanics and Their Application in Shale Hydraulic Fracturing: A Review. Journal of Petroleum Science and Engineering, 143, 158-170.

Zhang, Y., Zhang, J., Yuan, B., Yin, S. (2018). In-situ Stress Controlling Hydraulic Fracture

Propagation and Fracture Breakdown Pressure. Journal of Petroleum Science and Engineering, 164, 164-173.